Geochemistry, Geophysics, Geosystems

RESEARCH ARTICLE
10.1029/2020GC008914

Key Points:

- Seamounts are characterized by greater geochemical variability than the islands they surround, but resemble nearby islands
- Variations in seamount chemistry near Fernandina support that volcanoes undergo early evolutionary phases predicted by plume theory
- Patterns of geochemical/isotopic enrichment of seamounts within each region support fine scale mantle heterogeneities in the mantle source

Supporting Information:

- Supporting Information S1
- Table S1
- Table S2
- Table S3
- Table S4
- Table S5
- Table S6
- Table S7
- Table S8
- Table S9
- Table S10

Correspondence to:

D. M. Schwartz,
darinschwartz@boisestate.edu

Citation:

Schwartz, D. M., Wanless, V. D., Soule, S. A., Schmitz, M. D., & Kurz, M. D. (2020). Monogenetic near-island seamounts in the Galápagos Archipelago. *Geochemistry, Geophysics, Geosystems*, *21*, e2020GC008914. https://doi.org/10.1029/2020GC008914

Received 8 JAN 2020
Accepted 11 OCT 2020

Monogenetic Near-Island Seamounts in the Galápagos Archipelago

D. M. Schwartz[1], V. D. Wanless[1], S. A. Soule[2], M. D. Schmitz[1], and M. D. Kurz[3]

[1]Department of Geosciences, Boise State University, Boise, ID, USA, [2]Department of Geology and Geophysics, Woods Hole Oceanographic Institution, Woods Hole, MA, USA, [3]Department of Marine Chemistry and Geochemistry, Woods Hole Oceanographic Institution, Woods Hole, MA, USA

Abstract Rarely have small seamounts on the flanks of hotspot derived ocean-island volcanoes been the targets of sampling, due to sparse high-resolution mapping near ocean islands. In the Galápagos Archipelago, for instance, sampling has primarily targeted the subaerial volcanic edifices, with only a few studies focusing on large-volume submarine features. Sampling restricted to these large volcanic features may present a selection bias, potentially resulting in a skewed view of magmatic and source processes because mature magmatic systems support mixing and volcanic accretion that overprints early magmatic stages. We demonstrate how finer-scale sampling of satellite seamounts surrounding the volcanic islands in the Galápagos can be used to lessen this bias and thus, better constrain the evolution of these volcanoes. Seamounts were targeted in the vicinity of Floreana and Fernandina Islands, and between Santiago and Santa Cruz. In all regions, individual seamounts are typically monogenetic, but each seamount field requires multigenerational magmatic episodes to account for their geochemical variability. This study demonstrates that in the southern and eastern regions the seamounts are characterized by greater geochemical variability than the islands they surround but all three regions have (Sr-Nd-He) isotopic signatures that resemble neighboring islands. Variations in seamount chemistry from alkalic to tholeiitic near Fernandina support the concept that islands along the center of the hotspot track undergo greater mean depths of melting, as predicted by plume theory. Patterns of geochemical and isotopic enrichment of seamounts within each region support fine-scale mantle heterogeneities in the mantle plume sourcing the Galápagos hotspot.

Plain Language Summary Hotspots are places on Earth where volcanism occurs away from major plate boundaries and are, thus, not explained by the theory of plate tectonics. Instead, "plume theory" predicts that a least a portion of hotspot volcanism is related to the upwelling of hot mantle, which partially melts as it ascends and forms magma that produces ocean-island volcanoes. Chemistry of lavas sourced from these volcanoes are used to test predictions of the lifecycle of volcanoes, based on this theory, and understand chemical structure of the deep Earth. From a pragmatic perspective, a majority of the samples used to test plume theory are from the part of the islands that are exposed above the sea surface. We suggest that sampling restricted to these subaerial volcanic features may result in a biased view of magmatic and source processes. In this study we investigate whether finer-scale sampling of small submarine volcanoes surrounding the major islands in the Galápagos Archipelago can be used to more thoroughly test "plume theory." We show that seamounts exhibit greater chemical variability than the islands they surround. Samples from the seamounts align more closely with predictions of plume theory than island samples alone.

1. Introduction

Ocean islands form as a consequence of the intermittent eruption of lavas in a localized area as the Earth's lithosphere moves over a hotspot source (Wilson, 1963). Long-lived hotspot volcanism is most succinctly explained by the concept of so-called "plume theory" (Campbell, 2007; Morgan, 1971), which states that upwelling mantle "plumes," originating from the deep Earth, melt as they near the lithosphere, resulting in hotspot volcanism. "Plume theory" predicts linear volcanic chains that age in the direction of plate motion, relative to their fixed plume source. A single island or seamount contains an integrated history of repeated eruptions over a finite period of time (Morgan, 1971), whereas ocean island and seamount chains can collectively record hotspot activity occurring over tens-of-millions of years. As a result, ocean islands

and seamount chains can provide a remarkable long-term record of mantle source characteristics, crustal melt-storage and transfer, and eruption (Devey et al., 2003). These long-term records can be used to test detailed predictions of plume theory (Campbell, 2007) beyond basic age-progressive volcanic chains (Devey et al., 2003), which can be explained by other mechanisms (Courtillot et al., 2003). For example, a secondary test on plume theory is that volcanism resulting from an upwelling plume begins with low degrees of melting at its leading edge, which increases to an apex above the center of upwelling and is followed by lower extents of melting downstream, accompanied by waxing and waning volcanic intensity (Watson & McKenzie, 1991). This is predicted to cause melting at greater mean depths at the periphery of the plume due to a lower upwelling velocity than at its stem (Campbell, 2007). However, due to the difficulty in accessing the submarine portions of ocean island systems, the majority of the sampling of ocean island basalts (OIBs) has occurred on subaerial edifices or large submarine targets. This is potentially an issue since the extreme end-members of the OIB source are modified as melts mix (Stracke & Bourdon, 2009), evolve, and react during ascent and storage in the lithosphere prior to eruption at ocean islands (e.g., Peterson et al., 2014, 2017; Saal et al., 2007). Furthermore, ocean island volcanoes, being polygenetic in nature, are continuously erupting, and overprinting variations that arise during island growth (Devey et al., 2003). The potential for mixing in the mantle and crust, and resurfacing of the island, are greatest during the main stage of ocean island growth, where robust magma-supply favors the formation of shallow magma-reservoirs and large volume eruptions (e.g., Geist et al., 2014a). As a consequence, these highly processed lavas may dominate sampling even where volcanic edifices are dissected by erosion or mass wasting (e.g., Geist et al., 2002), leading to a selection bias. Thus, it is difficult to distinguish between ocean-island systems that lack origins consistent with the detailed predictions of plume theory and those that are inadequately sampled.

If there is a significant sample selection bias, we predict that: (1) plume-derived ocean islands should undergo an evolutionary sequence predicted by plume theory, with inconsistencies that represent oversampling of the main stage of formation, and (2) the length scales and magnitudes of mantle heterogeneity are finer and more extreme, respectively, than what is preserved in OIB due to magma mixing during ascent and storage in subisland magma chambers. The efficiency of this effect will be dependent on magma supply (i.e., completeness of lava flow cover), the arrangement of isotopic domains in the mantle and plate motion (e.g., Jones et al., 2017), and will be accentuated at ocean islands that are not extensively dissected by erosion or have less subaerial exposure. Furthermore, melting systematics introduced when there are multiple lithologies, with differing solidus temperatures, within a single mantle plume, can lead to burial of early erupted heterogeneities (Jones et al., 2017), which is tangentially related to the bias introduced by studying the mantle through ocean islands (e.g., Ito & Bianco, 2014; Stracke & Bourdon, 2009).

Smaller monogenetic cones are common features surrounding larger point-source volcanoes, and generally show greater chemical variability relative to one another than the larger edifice they surround (Brenna et al., 2011; Smith & Németh, 2017). Presumably, these smaller cones sample melts that ascend vertically and bypass the centralized magmatic system. As such, they potentially provide an alternative, punctuated record of source and storage conditions in a magmatic system (Wood, 1979). In ocean island systems, these features can be satellite cones or rift zones on a volcano flank or small seamounts on the submerged periphery of the volcanic island. Although the former is commonly targeted for sampling, these subaerial features are probably derived from the same central magma chamber feeding the larger volcano. The seamounts on the flanks of an ocean island volcano, given their peripheral location compared to similarly sized subaerial features, might instead originate from a reservoir isolated from that of an ocean island, providing a different perspective on the magmatic system. Thus, one approach to evaluating ocean island evolution and mantle heterogeneity on a finer scale is to sample lavas from near-island seamounts, which may not be overprinted during mainstage volcanism. Modern sonar systems have the ability to map, in detail, the shallow seafloor near ocean islands revealing innumerable constructive features, which previously eluded detection (e.g., Casalbore et al., 2018; Cousens & Clague, 2015; Greene et al., 2010; Schwartz et al., 2018a; Wanless et al., 2006a). The identification of these features provides an opportunity to test the significance of a sample selection bias.

We apply the concept of detailed intervolcano sampling at the Galápagos Archipelago, a hotspot sourced ocean-island system that does not conform to all aspects of traditional plume theory (Harpp & Geist, 2018). Interpretation of the origins of Galápagos volcanism is predominately based on geochemical analyses of

samples erupted on the subaerial volcanic islands (e.g., White et al., 1993), expansive submarine lava flows that form the platform terraces (Anderson et al., 2018; Geist et al., 2006, 2008), or dredging of massive seamounts offset from the currently active volcanic platform (Christie et al., 1992; Harpp & White, 2001; Hoernle et al., 2000; Sinton et al., 2014; Werner et al., 1999, 2003). Significant advances in our understanding of the Galápagos have come from investigations of the submarine system (long lava flows, platform studies, and northern Galápagos); however, these studies focus on large features on the periphery of the archipelago with limited investigations of submarine volcanic features on the top of the Galápagos Platform (Carey et al., 2016; Schwartz et al., 2018a). Here, we evaluate the importance of sample selection bias by investigating the distribution and geochemical heterogeneity of small near-island seamounts located throughout the modern archipelago. We present chemical and isotopic characterization of new samples from seamounts located in three regions, two of which are located on top of the platform and one on the leading edge of the plume. The lava compositions observed in each seamount region are compared to the adjacent volcanic islands to evaluate the relation between the seamounts and the main magmatic systems. Within this framework, we assess if seamount sampling extends the chemical and isotopic geography in each region, how this relates to the evolution of the Galápagos hotspot system, and the nature of heterogeneities in the Galápagos mantle source.

2. Background

2.1. Galápagos Island Evolution and Plume Theory

The Galápagos Archipelago is located on the Nazca Plate, approximately 200 km south of the Galápagos Spreading Center and 1,000 km off the west coast of South America (Figure 1). The Galápagos consists of 13 volcanic islands (McBirney & Williams, 1969) and numerous satellite constructions and seamounts (Figure 1; Schwartz et al., 2018a). Geophysical observations indicate that the Galápagos Islands are underlain by anomalously hot asthenosphere with an excess temperature of 30°C–150°C, attributed to the underlying Galápagos hotspot (Hooft et al., 2003; Villagomez et al., 2007, 2014). Basalts erupted at the western edge of the archipelago carry a chemical signature characteristic of an isolated primitive mantle reservoir ($^{3}He/^{4}He > 30$ R/R_A; Graham et al., 1993; Kurz & Geist, 1999; Kurz et al., 2009, 2014), suggesting that the hotspot results from upwelling and melting of a deeply seated mantle plume (Courtillot et al., 2003).

Galápagos Islands are most volcanically active on the western edge of the archipelago (Allan & Simkin, 2000) and increase in age with the direction of plate motion to the east (Geist et al., 2014b), consistent with their construction over a fixed source in the mantle (White et al., 1993; 51 km/Ma to the east; Argus et al., 2010) (Figure 1). Despite this general aging trend, islands remain volcanically active much longer than is predicted by plume theory alone, with historic eruptions distributed over an ~200 km-wide area on the islands of Fernandina, Floreana, Santiago and San Cristobal (Siebert et al., 2011). This prolonged volcanic activity has been explained by changes in lithospheric thickness across the archipelago that is not observed in Hawai'i (Feighner & Richards, 1994; Gibson & Geist, 2010) and interaction of the hotspot with a mid-ocean ridge to the north (Cleary et al., 2020; Colin et al., 2011; Cushman et al., 2004; Detrick et al., 2002; Kelley et al., 2013; Kokfelt et al., 2005), which may enhance volcanic activity downstream from the center of upwelling (Harpp et al., 2003; Harpp & Geist, 2002, 2018; Mittelstaedt et al., 2012).

Unlike many other ocean island systems, the volcanic islands in the modern Galápagos Archipelago are underlain by a large, shallow submarine platform (Geist et al., 2006, 2008). The platform has nearly 4,000 m of vertical relief in the west, at the leading edge of the hotspot, and represents the majority of erupted material in the archipelago. Platform construction is thought to have occurred through eruption of large-volume tholeiitic lava-flows that preceded island formation above the leading edge of the plume (Geist et al., 2008). If true, this suggests that either (i) the earliest phase of volcanism in the Galápagos differs significantly from that of prototypical hotspot evolution, where initial island building begins with low-volume, preshield building, alkalic magmatism (Clague & Dalrymple, 1987) or (ii) the evidence of this phase has been buried by subsequent volcanism. Recent analysis of long lava-flows extending west of the platform are alkalic and are attributed to low degrees of partial melting (Anderson et al., 2018). It is unclear how exactly these sparse alkalic flows relate to island formation along the central hotspot track. One possibility is that the absence of a clear preshield phase results from inadequate sampling above the leading edge of the plume.

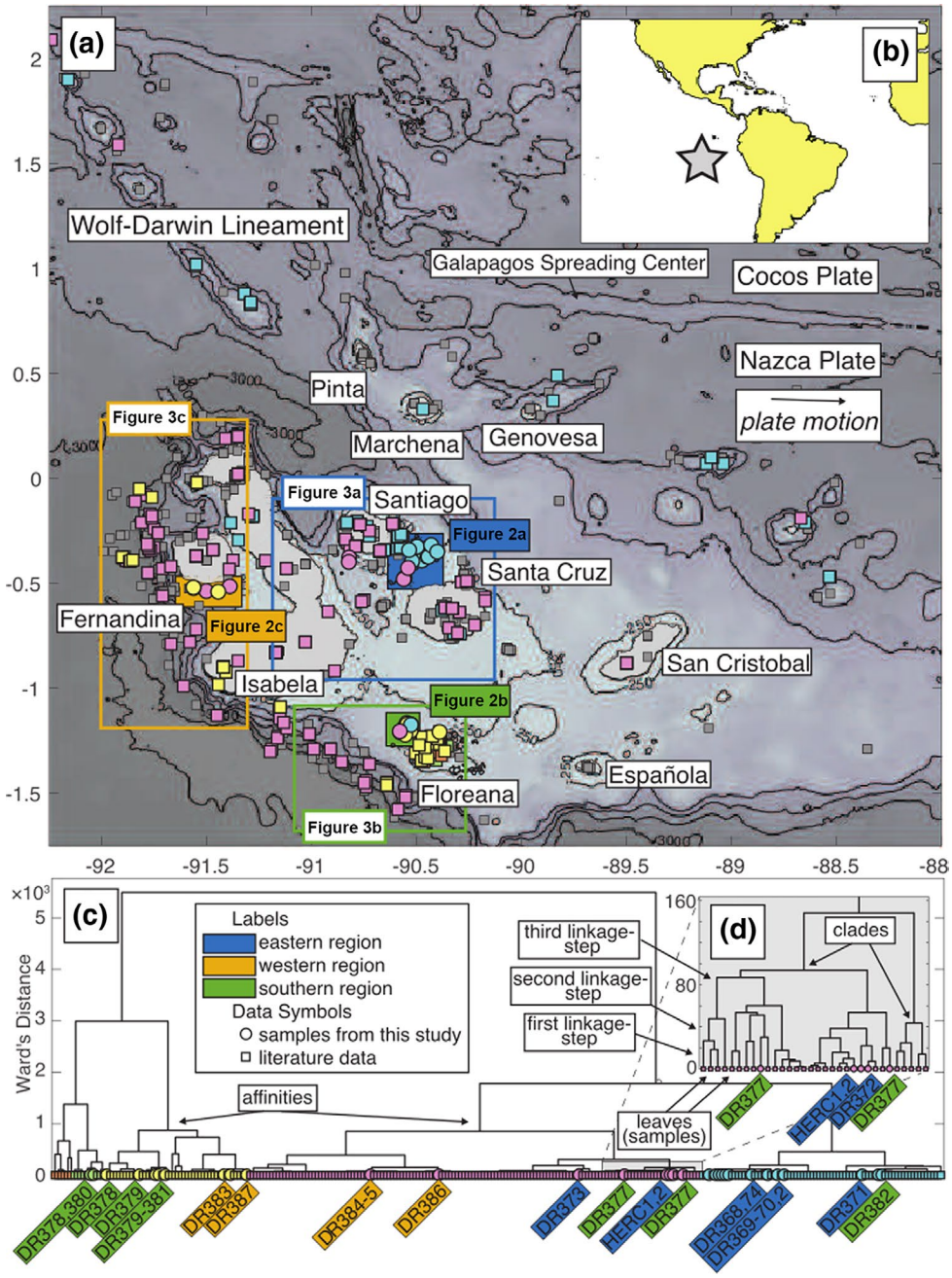

Figure 1. a) Map of the Galápagos Archipelago, with islands are shown in green. Literature sample locations are shown as colored squares (see Section 3.5 for data sources). Samples from this study are shown as colored circles. Samples are colored by agglomerative clustering into five affinities based on similarities in trace element and isotopic ratios (see panel c and Section 3.5 for more details). Samples from literature data that do not include all of the elements and isotope ratios used in the clustering analysis are gray (see Table 1 for data sources). Bathymetric contour interval is 500 m except the shallowest index at 250 m, data from Ryan et al. (2009). Filled colored boxes show the locations of panels in Figure 2. Open colored boxes show the locations of panels in Figure 3. Nazca Plate motion, relative to the fixed hotspot reference frame is nearly due east and is shown as a black arrow in the bottom left of the map (Argus et al., 2010). (b) Gray star shows the location of the Galápagos Archipelago. (c) Dendrogram showing results of the regional agglomerative clustering analysis. Samples from this study are indicated by the color flags corresponding to their regional colors in panel a and labeled by seamount. Samples are ordered by their similarity within each affinity (see Section 3.5 for more details) (d) Select portion of the dendrogram, enlarged to show details. Individual samples are shown as leaves at the bottom of the diagram. The first three linkage-steps for the leaf on the far left of the diagram, and its subsequent clades, are indicated with arrows. Clades are any group of samples within the dendrogram, with examples labeled in the figure inset.

2.2. Isotopic Zonation of the Galápagos Plume

Since its early expression in the Caribbean Large Igneous Province (~90 Ma; Gazel et al., 2018; Geldmacher et al., 2003), the Galápagos hotspot has produced lavas of four geochemical types with the same spatial distribution of distinct isotopic domains reflected at the surface for >70 Ma (Buchs et al., 2016; Geldmacher et al., 2003; Gazel et al., 2018; Hauff et al., 2000; Hoernle et al., 2000; Harpp et al., 2014a; Trela et al., 2015; White et al., 1993; Werner et al., 2003). In general, individual islands (especially those in the west), seamounts, and submarine lava flows are typified by eruption of relatively limited lava compositions compared to the geochemical diversity observed on the archipelago scale (White et al., 1993). Based on radiogenic isotope ratios, the zonation of the Galápagos mantle plume is commonly described as a horseshoe with an enriched and a depleted interior (Geist et al., 1988; White & Hofmann, 1978; Figure 1). In the modern archipelago, different endmember components contributing to these domains have been defined through principle component analysis and are commonly referred to as PLUME (given its predominance at the center of "plume" upwelling), FLO (short for "Floreana") and depleted upper-mantle (DUM), and Wolf-Darwin Lineament (WDL) (Harpp & White, 2001). The unique zonation pattern, consisting of the highest contributions from enriched PLUME material to the west, FLO to the south and DUM to the east, has been attributed to entrainment of upper mantle into a gradationally-zoned plume during ascent (Blichert-Toft & White, 2001; Harpp & White, 2001; White et al., 1993), plume-ridge interaction (Gibson et al., 2015; Ito & Bianco, 2014), or tapping of a complexly zoned or striped plume (Gazel et al., 2018; Gibson et al., 2012; Harpp et al., 2014a; Hoernle et al., 2000; Werner et al., 2003; White et al., 1993). Helium isotopic variations also show strong geographical zonation, with Fernandina as the most distinct high $^{3}He/^{4}He$ endmember (Kurz et al., 2009; Kurz & Geist, 1999). Other models suggest that isotopic heterogeneities are much shorter, on the kilometer scale or less (e.g., Harpp et al., 2014b). Regardless of the exact origins of the mantle heterogeneities, almost all studies invoke models of the mantle that have unevenly distributed portions of the principle component endmembers described by Harpp et al. (2001), that are preferentially sampled by the various islands in a geographically coherent way.

If the large edifice sampling selection bias has played a significant role in the formulation of the domain model (Hoernle et al., 2000), then sampling on a finer scale should resolve more extreme variation in the trace element and isotopic compositions of erupted lavas. Fine-scale sampling provides an opportunity to test whether or not isotopic domains represent greater portions of the endmembers represented by the principle components identified by Harpp and White (2001). At the very least, higher resolution sampling can be used to investigate the extent to which the apparent domains are a mixture of different proportions of all endmembers identified as principle components by Harpp and White (2001). If selection bias is insignificant, then all seamount samples will be of a similar composition to the domain represented in each region or that of a previously sampled upstream domain.

3. Methods

3.1. Seamount Mapping, Sampling and Initial Sample Preparation

In 2015, two research cruises on the E/V *Nautilus* and M/V *Alucia* mapped >100 seamounts on the top of the Galápagos Platform, most of which were previously undiscovered (Carey et al., 2016; Schwartz et al., 2018a, 2018b). Approximately 150 rock samples were collected from the seamounts using the Ocean Exploration Trust's remotely operated vehicle *Hercules* and the Dalio Foundation's human occupied submersibles *Deep Rover 2* and *Nadir* (Table S1). The seamounts visited in this study are referred to by their corresponding *Deep Rover 2* dive number (e.g., DR366). Seamounts around three islands were targeted: south and southeast of Santiago, northwest of Floreana, and south of Fernandina (Figure 1; Table 1). These regions were chosen based on satellite altimetry derived bathymetry that suggested the presence of seamounts (Ryan et al., 2009), and because they contain basalts with characteristics that represent three of the primary geochemical endmembers (PLUME, DUM, and FLO) in the archipelago (e.g., Harpp et al., 2001).

The seamounts were mapped at 10 m spatial resolution by shipboard multibeam (Schwartz et al., 2018a, Figure 2). Once mapped, seamounts were targeted that displayed variable morphology (e.g., elongation direction, aspect ratio; surface roughness, and volume) in order to increase the likelihood of sampling unique volcanic events and to test whether there is any systematic relationship between seamount morphology

Table 1
Summary of Geochemical and Morphological Data by Region and Seamount

Seamount sample	Vol. (km^3)	Aspect ratio	Elong. dir.	MgO	K_2O+Na_2O	$[La/Sm]_N$	$[Sm/Yb]_N$	87Sr/86Sr	143Nd/144Nd
Eastern region	**6.4**			***6.8(3.2)***	***4.0(1.6)***	***1.6(0.7)***	***2.1(0.6)***	***0.70301(25)***	***0.51303(6)***
Seamounts	**0.07**	**1.7**	**96**	**8.9(1.1)**	**2.8(0.3)**	**1.1(0.3)**	**1.8(0.4)**	**0.70281(10)**	**0.51305(3)**
DR366	**0.35**	**1.7**	**82**	**9.25**	**2.65**	**0.87**	**1.48**	**0.702787**	**0.513054**
AL150801-007				9.25	2.48	0.81	1.40		
AL150801-006				8.44	2.80	0.88	1.49		
AL150801-005				10.1	2.50	0.88	1.50	0.702741	0.513068
AL150801-004				8.58	2.83	0.90	1.54		
AL150801-003				9.72	2.54	0.89	1.50		
AL150801-001				9.42	2.76	0.88	1.47	0.702834	0.513040
DR367	**0.39**	**2.0**	**90**	**8.98**	**2.63**	**0.82**	**1.62**	**0.702652**	**0.513082**
AL150801-016				10.1	2.73	0.84	1.65	0.702665	0.513085
AL150801-013				8.06	2.51	0.82	1.56		
AL150801-012				8.81	2.67	0.82	1.64	0.702639	0.513078
AL150801-011				8.93	2.61	0.82	1.62		
DR368	**0.35**	**1.5**	**118**	**9.74**	**2.54**	**0.93**	**1.45**	**0.702827**	**0.513056**
AL150801-029				9.54	2.52	0.93	1.44		
AL150801-028				10.2	2.63	0.96	1.51		
AL150801-027				10.6	2.44	0.92	1.44	0.702827	0.513056
AL150801-026				9.05	2.55	0.90	1.46		
AL150801-025				9.81	2.47	0.92	1.46		
AL150801-024				9.94	2.59	0.95	1.48		
AL150801-023				9.50	2.54	0.91	1.42		
AL150801-022				9.28	2.57	0.91	1.42		
DR369-70	**0.13**	**1.2**	**100**	**8.95**	**2.63**	**0.93**	**1.53**	**0.702709**	**0.513070**
AL150801-034				8.95	2.63	0.93	1.53	0.702709	0.513070
DR371	**0.11**	**1.1**	**138**	**9.12**	**2.97**	**1.07**	**1.78**	**0.702717**	**0.513081**
AL150801-036				9.12	2.97	1.07	1.78	0.702717	0.513081
DR372	**0.38**	**1.4**	**1**	**7.74**	**2.80**	**1.13**	**1.54**	**0.702870**	**0.513047**
AL150801-045				7.66	2.55	0.90	1.36		
AL150801-043				6.52	2.60	0.89	1.49		
AL150801-042				8.69	2.59	0.91	1.47	0.702867	0.513050
AL150801-039				8.26	2.50	0.96	1.48	0.702832	0.513037
AL150801-038				7.59	3.25	1.59	1.65		
AL150801-037				7.70	3.33	1.55	1.78	0.702911	0.513054
DR373				**5.11**	**3.63**	**1.56**	**2.39**	**0.702888**	**0.513056**
AL150801-048				5.11	3.63	1.56	2.39	0.702888	0.513056
DR374	**0.35**	**1.5**	**126**	**10.48**	**2.38**	**0.77**	**1.31**	**0.702846**	**0.513053**
AL150801-055				10.1	2.42	0.80	1.35		
AL150801-052				10.5	2.37	0.76	1.30		
AL150801-051				10.9	2.35	0.76	1.30	0.702846	0.513053
DR375	**0.024**	**1.1**	**90**	**8.66**	**3.08**	**1.05**	**1.63**	**0.702746**	**0.513078**
AL150801-058				8.57	3.03	1.05	1.64		

Table 1 *(continued)*

Seamount sample	Vol. (km^3)	Aspect ratio	Elong. dir.	MgO	K_2O+Na_2O	$[La/Sm]_N$	$[Sm/Yb]_N$	87Sr/86Sr	143Nd/144Nd
AL150801-057				8.46	3.14	1.04	1.62		
AL150801-056				8.95	3.06	1.05	1.62	0.702746	0.513078
HERC1	**0.30**	**1.3**	**57**	**8.50**	**3.22**	**1.47**	**2.32**	**0.702996**	**0.513004**
NA-064-114				8.64	3.16	1.51	2.30		
NA-064-115				8.35	3.13	1.45	2.26		
NA-064-116				8.10	3.22	1.45	2.21		
NA-064-120				8.88	3.26	1.48	2.35		
NA-064-123				8.17	3.32	1.46	2.38		
NA-064-127				8.36	3.23	1.47	2.34		
NA-064-129				8.99	3.24	1.48	2.37	0.702996	0.513004
HERC2	**0.60**	**1.1**	**5**	**8.70**	**3.22**	**1.49**	**2.41**	**0.702917**	**0.513001**
NA-064-131				9.42	3.11	1.45	2.32	0.702917	0.513001
NA-064-132				8.87	3.27	1.51	2.43		
NA-064-133				7.74	3.06	1.47	2.28		
NA-064-134				8.77	3.35	1.52	2.55		
NA-064-135				8.70	3.30	1.51	2.46		
Southern region	**5.7**			***9.2(4)***	***3.5(0.9)***	***3.1(1)***	***1.8(0.3)***	***0.70340(22)***	***0.51294(2)***
Seamounts	**0.09**			**9.7(2)**	**3.0(0.5)**	**3.1(1)**	**1.7(0.2)**	**0.70340(14)**	**0.51296(2)**
DR377	**0.56**	**1.1**	**152**	**8.00**	**2.55**	**2.22**	**1.56**	**0.703296**	**0.512963**
AL150801-070				8.80	2.44	2.24	1.55		
AL150801-069				9.27	2.25	2.24	1.54	0.703294	0.512965
AL150801-067				8.14	2.57	2.15	1.61		
AL150801-066				8.44	2.60	2.27	1.55	0.703298	0.512961
AL150801-065				5.35	2.88	2.19	1.55		
DR378	**0.18**	**1.4**	**179**	**10.71**	**3.55**	**4.70**	**1.77**	**0.703572**	**0.512940**
AL150801-080				10.8	3.08	4.78	1.78	0.703435	0.512937
AL150801-076				11.5	4.07	4.66	1.77	0.703710	0.512942
AL150801-073				9.73	3.49	4.66	1.77		
DR379	**0.043**	**1.5**	**39**	**9.31**	**2.21**	**3.26**	**1.57**	**0.703429**	**0.512954**
AL150801-089				9.55	2.56	3.31	1.60	0.703413	0.512955
AL150801-088				6.90	1.93	3.30	1.74		
AL150801-084				11.5	2.14	3.16	1.37	0.703446	0.512952
DR380A	**0.15**	**1.2**	**160**	**10.23**	**3.40**	**3.26**	**2.14**	**0.703282**	**0.512957**
AL150801-094				10.7	3.42	3.31	2.12		
AL150801-093				11.0	3.34	3.25	2.13	0.703282	0.512957
AL150801-092				9.00	3.45	3.24	2.18		
DR380B	**0.15**	**1.2**	**160**	**10.82**	**3.42**	**4.92**	**1.74**	**0.703596**	**0.512936**
AL150801-099b				10.7	3.18	4.87	1.75		
AL150801-099				10.5	3.45	4.96	1.74		
AL150801-098b				11.2	3.41	5.04	1.71	0.703596	0.512936
AL150801-098				10.9	3.64	4.82	1.75		
DR381	**0.50**	**1.3**	**179**	**10.55**	**3.44**	**2.49**	**1.93**	**0.703328**	**0.512957**
AL150801-106				10.1	3.55	2.58	1.93		

Table 1 *(continued)*

Seamount sample	Vol. (km^3)	Aspect ratio	Elong. dir.	MgO	K_2O+Na_2O	$[La/Sm]_N$	$[Sm/Yb]_N$	87Sr/86Sr	143Nd/144Nd
AL150801-105				11.0	3.33	2.41	1.93	0.703328	0.512957
DR382	**0.043**	**1.4**	**0**	**9.62**	**2.75**	**1.46**	**1.48**	**0.703321**	**0.512995**
AL150801-112				8.84	2.96	1.45	1.50		
AL150801-111				11.3	2.71	1.51	1.39	0.703334	0.513000
AL150801-109				10.1	2.55	1.43	1.48	0.703308	0.512989
AL150801-108				8.20	2.79	1.46	1.54		
Western region	**1.2**			***6.4(3)***	***3.6(0.7)***	***1.8(0.8)***	***2.7(0.7)***	***0.70316(19)***	***0.51296(4)***
Seamounts	**0.06**			**5.9(0.6)**	**4.4(1)**	**2(0.3)**	**3.1(0.4)**	**0.70325(1.4)**	**0.51296(2)**
DR383	**0.44**	**1.4**	**5**	**5.24**	**5.27**	**2.21**	**3.46**	**0.703239**	**0.512974**
AL150801-128				4.88	5.39	2.20	3.49		
AL150801-127				5.41	5.13				
AL150801-126				5.31	5.31	2.19	3.41		
AL150801-125				5.24	5.25	2.20	3.59		
AL150801-124				4.97	5.24	2.23	3.38		
AL150801-123				5.47	5.22	2.21	3.49	0.703239	0.512974
AL150801-120				5.38	5.29	2.22	3.40	0.703239	0.512974
AL150801-119				5.24	5.36	2.24	3.45		
DR384-5	**0.22**	**1.1**	**90**	**6.51**	**3.03**	**1.69**	**2.65**	**0.703256**	**0.512938**
AL150801-131				6.19	3.04	1.63	2.67		
AL150801-130				6.32	3.12	1.71	2.56	0.703241	0.512944
AL150801-129				6.88	2.83	1.70	2.66		
DR386	**0.020**	**6.6**	**123**	**6.65**	**3.11**	**1.74**	**2.70**	**0.703271**	**0.512931**
AL150801-138				6.78	3.08	1.72	2.67	0.703271	0.512931
AL150801-137				6.56	3.12	1.74	2.76		
AL150801-134				6.69	3.11	1.74	2.69		
AL150801-133				6.56	3.14	1.75	2.68		
AL150801-132				6.36	3.17	1.69	2.66		
DR387	**0.14**	**1.1**	**88**	**6.05**	**4.84**	**2.25**	**3.34**	**0.703258**	**0.512971**
AL150801-148				5.90	4.92	2.27	3.31		
AL150801-147				6.06	4.89	2.27	3.37		
AL150801-146				6.04	4.86	2.28	3.38		
AL150801-145				6.19	4.79	2.22	3.28	0.703258	0.512971
AL150801-144				6.02	4.81	2.21	3.32		
AL150801-141				6.08	4.75	2.22	3.37		

Note. Data in bold is the average of each seamount and seamount region. Numbers in italics are averages for the literature data eastern region (Bailey, 1976; Baitis and Lindstrom, 1980; Baitis and Swanson,1976; Blichert-Toft & White, 2001; Cox & Dalrymple, 1966; Geist et al., 1985, 1994, 1995, 2008; Gibson and Geist, 2010; Gibson et al., 2012; Handley et al., 2011; Hedge, 1978; Koleszar et al., 2009; M. D. Kurz and Geist, 1999; Macdonald et al., 1992; McBirney & Williams, 1969; McBirney et al., 1985; Puzankov & Bobrov, 1997; Reynolds & Geist, 1995; Righter et al., 1998; Saal et al., 2007; Shimizu et al., 1981; Swanson et al., 1974; White et al., 1993; Wilson, 2013), southern region (Al, 2000; Blichert-Toft & White, 2001; Bow & Geist, 1992; Chaussidon & Marty, 1995; Christie, 2004; Cox & Dalrymple, 1966; D. J. Geist et al., 2008; Graham et al., 1993; K. Harpp et al., 2014b; K. S. Harpp and White, 2001; Kurz & Geist, 1999; Lyons et al., 2007; Marty & Humbert, 1997; McBirney & Williams, 1969; Peterson et al., 2017; Saal et al., 2007; Shimizu et al., 1981; Turner et al., 2006; White et al., 1993; Yi et al., 2000) and western region (Anderson et al., 2018; Bailey, 1976; Blichert-Toft & White, 2001; Chaussidon & Marty, 1995; Christie, 2004; Cox & Dalrymple, 1966; D. Geist et al., 1998; D. Geist et al., 2002; D. J. Geist et al., 2005; D. J. Geist et al., 2006; Graham et al., 1993; Handley et al., 2011; K. S. Harpp and White, 2001; Jackson & Carlson, 2012; Koleszar et al., 2009; Kurz & Geist, 1999; M. D. Kurz et al., 2009; Liang et al., 2017; Marty & Humbert, 1997; McBirney & Williams, 1969; Naumann et al., 2002; Nusbaum et al., 1991; Peterson et al., 2017; Pringle et al., 2016; Raquin & Moreira, 2009; Saal et al., 2007; Shimizu et al., 1981; Standish et al., 1998; Teasdale et al., 2005; White et al., 1993) as identified in Figure 1 and shown in detail in Figure 3. Numbers in parentheses are 1 SD of the values used for each average. Average spatial statistics from each region are averaged from Table S2.

and composition. Postcruise, morphological characteristics were quantified using seamount footprints and bathymetric data (Schwartz et al., 2018a). Seamount volume was calculated as the difference between the mean depth of all the pixels within each seamount and mean base depth of each seamount, converted to volume by multiplying this value by the number of pixels comprising the seamount and individual pixel area. Similarly, the volume of the subaerial portion of Santiago, Floreana, and Fernandina islands were calculated for reference with a global multiresolution topography grid (Ryan et al., 2009), using the mean elevation of each island. Aspect ratio is calculated as the length divided by normally oriented width of each seamount (L/W), in the orientation that maximized this value. The direction of the long axis in the aspect ratio measurement was further recorded as the elongation direction (Table S2).

Submersible dives typically began at the base of each seamount and collected samples up the seamount's stratigraphy to assess the chemical variability within a single seamount. Upon recovery, samples were rinsed and cleaned of biological residue and air dried. At Boise State University (BSU) rock samples were further crushed by sledge and ceramic plate jaw crusher to 1–10 mm diameter chips. Chips were sonicated three times in an ultrasonic bath with ultrapure 18.2 megaohm H_2O to remove contaminants, leached in the ultrasonic bath for 20 min with 1% hydrogen peroxide, and finally rinsed three times with ultrapure H_2O to remove alteration products and surficial seawater contamination.

3.2. Major and Trace Element Analysis

Fresh chips of basalt, devoid of alteration, were hand-picked under binocular microscope for analysis, typically from the 5–10 mm size fraction. Cleaned chips (10–20 g) were powdered at Washington State University (WSU) Geoanalytical Facility using a swing mill with tungsten carbide surfaces. Powders were double fused with Li-tetraborate into a glass bead for analysis. X-ray fluoresence (XRF) analysis was carried out in four sessions using a Thermo-ARL automated XRF spectrometer at WSU under the methods of Johnson et al. (1999; Table S3). Reproducibility of major elements was assessed by repeat measurements of unknowns, which was between 0.25% and 1% for all oxides except K_2O (2.8%) (Table S4). Although we collected a comprehensive suite of trace elements by inductively-coupled plasma mass-spectrometry (ICP-MS) for all samples analyzed for XRF, we additionally report select high abundance trace element concentrations obtainable by XRF. Loss on ignition (LOI) was measured for all samples. High LOI is taken as an indication of high degrees of alteration or significant adhering carbonates. Samples with LOI >1% are not interpreted with the rest of the major element data and are flagged with an "X" in the major element diagrams and subsequently described trace element results.

For all samples analyzed for major elements, an additional 50 mg of material was handpicked from the 1–2 mm size fraction for solution ICP-MS trace element analysis. Care was taken to select chips without obvious phenocrysts, alteration, or adhering carbonates. Picked separates were further sonicated in ultrapure H_2O for 20-min intervals, with fines decanted in-between, until clear. Samples were dissolved in 15 ml Savillex PFA beakers following the procedure of Kelley et al. (2003) and Lytle et al. (2012), as modified and summarized in Schwartz et al. (2018b). Trace element concentrations were measured in three sessions on diluted aliquots (2500X) of dissolved samples and standards over the course of a year, using a Thermo Electron X-Series II Quadrupole ICP-MS coupled with an Elemental Scientific Inc. (ESI) SC-FAST solution autosampler at BSU. Concentrations were calibrated from the instrumental raw-counts using the Geological and Environmental Reference Material (GeoReM) preferred values for United States Geological Survey standards Hawaiian Volcano Observatory Basalt, Icelandic Basalt, Diabase (W-2)(Jochum et al., 2016); and basalt from the Geological Survey of Japan (JB-3) and dolerite (DNC-1)(GeoReM accepted values), tied at the y-intercept to a total procedural blank measurement. Individual analyses (30 s) were adjusted to a uniform sensitivity using a 20 ppb In internal standard solution. Final concentrations were determined by the average of three analyses, and analytical precision was determined from the standard deviation of these runs (Table S5). All data reduction to this point was carried out using PlasmaLab software. Repeat measurements of JB-3 were made every 5–10 analyses to monitor and correct for instrumental drift (averaged percent relative deviation of JB-3 drift measurements from initial calibration value, calculated block by block; <1% correction on average for all blocks).

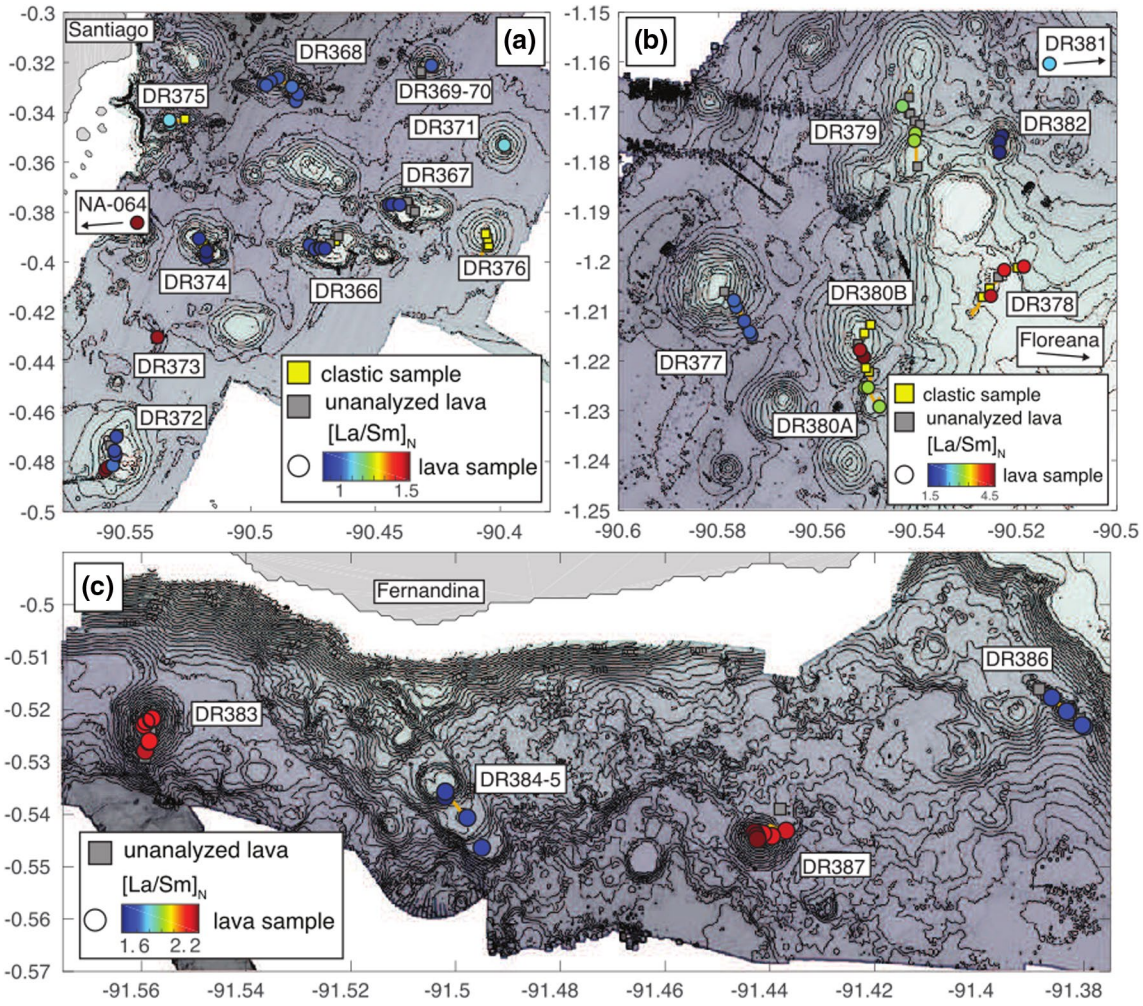

Figure 2. Map of seamount samples for eastern (a), southern (b), and western regions (c). Labels indicate human occupied submersible dive names. Gold lines show submersible dive track. Clastic samples are shown as yellow squares. Lavas that were not analyzed because of high degrees of alteration are shown as gray squares. All other samples are shown as colored circles representing $(La/Sm)_N$ (Table 1).

Precision of the ICP-MS data is given by the reproducibility of geologic standards (and repeat measurements of samples) measured before and after each session (Table S6). These uncertainties are typically 2%–5% for all elements >0.5 ppm, which is comparable to the internal precision of the three averaged analyses (Table S7). Of note, reproducibility of high abundance transition metals for our XRF analyses is a factor of 5 better than on the ICP-MS (1%; Ni, Cr, V), and comparable for lower abundance elements (2%–4%; Sc, Ga, Cu, Zn). Thus, we prefer these XRF derived measurements for these elements over the ICP-MS values.

3.3. Radiogenic Isotope Analysis

Splits of the chipped samples, previously prepared for major and trace element analysis, were leached in 6 M HCl to remove the effect of seawater contamination and alteration on the isotopic ratios. To assess the effects of alteration and contamination on the measured isotopic ratios, samples were leached using two methods, the first was a gentle approach and involved the repeat leaching of samples in an ultrasonic bath (e.g., Nobre Silva et al., 2009); the second was more aggressive, where samples were leached for two 3-h periods in 150°C 6M HCl, followed by repeated 20 min sonication in ultrapure H_2O and decanting until clear of fines. Leached rock chips were dissolved and separated into their chemical species using ion exchange chromatography, using standard procedures practiced at the BSU Isotope Geology Laboratory (IGL; Fisher

et al., 2011; Sousa et al., 2013) as adapted from Korkisch and Worsfold (1990). All isotope ratios were measured on the IsotopX Phoenix X62 thermal-ionization mass spectrometer at the IGL.

Strontium isotope ratios were measured on single Re filaments in a three-sequence dynamic routine utilizing five Faraday cups (e.g., Kurz et al., 2017). Samples were loaded using 2 μL Ta gel emitter solution following standard loading procedures. Samples and standards were run maintaining 2–4V ^{88}Sr beam for 150 cycles. Internal precisions of analyses are typically 6–12 ppm (2SE) for ^{87}Sr/^{86}Sr (Table S8). Mass dependent fractionation is corrected using an exponential law and ^{86}Sr/^{88}Sr of 0.1194. The mean of National Bureau of Standards -987, used as a check standard for this analytical session is 0.710247 ± 8 (11 ppm 2 SD, n = 31), which is within error of the accepted value of 0.710248 ± 23 (Thirlwall, 1991). Thus, no bias or detectable blank were observed or corrected for in our data.

Neodymium isotope ratios were measured using a triple filament setup, with sample loaded on a single side filament and ionized from a high temperature center filament (Thirlwall, 1982). Analysis comprised a three-sequence dynamic routine utilizing five Faraday cups (e.g., Kurz et al., 2017). Samples were loaded as 3 μL aliquots of dilute nitric acid. Samples and standards were run maintaining ≥2V ^{144}Nd beam for 150 cycles. Internal precisions of analyses are 20 ppm (2SE) on average for ^{143}Nd/^{144}Nd (Table S8). Mass dependent fractionation is corrected using an exponential law and ^{146}Nd/^{144}Nd = 0.7219. The mean of JNdi-1 ^{143}Nd/^{144}Nd, used as a check standard for this analytical session is 0.512104 ± 4 (7 ppm 2 SD, n = 34); between run reproducibility is consistently better than the internal precision of analyses (Table S8). The mean of measured JNdi-1 is within error of the consensus value for JNdi-1 of 0.512115 ± 7 (Tanaka et al., 2000). Similar to Sr, given the similarity of check standard measurements and the accepted value of JNdi-1, no bias or detectable blank were observed or corrected for in these data.

3.4. He Isotope Analysis

Olivine grains used for He isotopic analysis were handpicked under a binocular microscope, from the 500–1,000 μm sieve fractions of crushed and cleaned samples. Helium measurements of crushed and melted olivine samples were carried out at Woods Hole Oceanographic Institution using the fully automated mass spectrometer system (MS2), consisting of a 90° magnetic sector helium isotope mass spectrometer and a quadrupole mass spectrometer on the extraction line for pre-measurement of gases. The analyses followed the analytical procedure described by Kurz and Geist (1999), Kurz (1986a), and Kurz et al. (1996). Crushing the olivine in vacuum releases He contained in melt and fluid inclusions, which is representative of the inherited magmatic component and measured as ^{3}He/^{4}He (Kurz 1986b), and reported as the ^{3}He/^{4}He relative to the present day atmospheric ratio (R/R_A). Melting the crushed fraction in a single step releases the remaining gas, yielding total concentrations of ^{3}He and ^{4}He. We also report isotopic ratios obtained upon melting, which were initially collected to assess the presence of a cosmogenic component, originating from subaerial sample exposure (Schwartz et al., 2018a), reported in Table S9. The similarity of crushed and melted isotopic compositions demonstrate that the samples did not accrue significant cosmic radiation while above the sea surface, are not discussed further. We assume that the inherited He ratio does not change due to the radiogenic production of ^{4}He from the decay of U and Th. This assumption is valid due to the relatively young eruption ages and low concentration of U and Th in the samples (<1 ppm; Table S5).

3.5. Agglomerative Clustering Analysis

To statistically compare the new seamount data between itself and previously existing data, we have performed two hierarchical-clustering analyses of the combined seamount and regional dataset. The first analysis is used to exhibit the archipelago-wide geochemical variations and how this relates to seamount compositions (Figure 1). The second examines how the seamounts vary within themselves and between proximal islands or other features sampled within each region as defined by the map extents in each panel of Figure 3, which are the same as the colored outlines of Figure 1a. The hierarchical clustering analysis is meant to allow for the visual assessment of the similarity or difference between one another and the literature data from the region. Differing from the principle component analysis of Harpp and White (2001), we

choose to use isotopic and trace element characteristics, which are sensitive to both source and degree of melting, which likely both vary across the archipelago (Gibson & Geist, 2010; White et al., 1993).

The archipelago-wide and regional clustering analyses utilize the MATLAB™ function *linkage*, which is an agglomerative hierarchical clustering analysis. The function *linkage* is based on a separate function *pdist*, which measures the distance (i.e., dissimilarity) between pairs of observations. For this analysis, these distances are derived from all of the trace element ratio permutations resulting from select trace elements (La, Ce, Nd, Sm, Yb, Th, Nb, and Ba), and isotope ratios ($^{87}Sr/^{86}Sr$ and $^{143}Nd/^{144}Nd$). The trace elements were chosen due to their relatively high concentration and utility in distinguishing between source characteristics defined previously, including rare-earth element patterns and Th, Nb, and Ba anomalies (e.g., Harpp and White, 2001). Of note, the use of these specific elements and isotope ratios limits the seamount and comparison dataset to samples that have all of this data, which filters the dataset to more recent publications, especially those reporting trace elements (Anderson et al., 2018; Christie et al., 2004; Fisk et al., 1982; Geist et al., 2002, 2008; Gibson et al., 2012; Graham et al., 1993; Handley et al., 2011; Kelley et al., 2013; Kurz & Geist, 1999; Marty & Humbert, 1997; Naumann & Geist, 2002; Peterson et al., 2017; Saal et al., 2007; Schilling et al., 2003; Sinton et al., 2014; Wilson, 2013). We have chosen to not include He isotopic composition in the clustering analysis because it would considerably limit the seamount and comparison dataset.

The *pdist* function uses the Ward Method to determine the distance between samples in the dendrograms. The Ward Method combines samples and clusters where a merger results in the least overall increase of resulting within-cluster variance, or Ward's Distance. The Ward's Distance is the inner squared Euclidian distance between all samples within clusters and is visualized as the length of the vertical lines connecting leaves in the resulting dendrogram. In the agglomerative clustering algorithm, samples linked within the first linkage step, shown at the bottom of the dendrogram (Figure 1d), are the most similar, and dissimilarity increases at higher linkage steps. For visualization, samples are clustered into five colored-clades for all analyses, which we refer to as "affinities." As opposed to the initial linkage of samples, affinities are selected from the "top down," splitting clades separated by the greatest Ward's Distance until five affinities are segregated. However, we note that despite using a clustering approach for determining affinities, which are used to visually assess the similarities and differences between samples, pairs are ordered within each cluster by the function *optimalLeafOrder*, which maximizes the sum of the similarities between adjacent samples by flipping tree branches without dividing clusters. So, in this way, the similarity between all samples can be assessed independent of their designated affinity (Figures 1 and 3).

4. Results

Summaries of the seamount spatial statistics, including rose diagrams of seamount elongations and histograms for the seamount volume and aspect ratio for each region, are shown in Figure S1 and described by region below (Table S2). A total of 145 rock samples were recovered from 21 seamounts. Many of the samples were variably altered and contaminated by adhering carbonates on outer surfaces and in vesicles. From the eastern and southern regions, 20 samples were volcaniclastic (termed "clastic") and are not evaluated further (Figure 2). Only samples reasonably cleaned of alteration were analyzed for major and trace elements ($N = 81$), and subsequent isotopic analysis ($N = 31$). The majority of our samples were recovered using the M/V *Alucia*, but we include in our discussion 13 samples collected on the R/V *Nautilus* (Anderson et al., 2018; Schwartz et al., 2018b) since three of these samples were analyzed for isotopes and are presented in this study. Trace elements from Schwartz et al. (2018b) have been reprocessed using updated standard values and reported here, so they can be compared directly with our data.

Excluding samples with LOI >1%, all samples analyzed are tholeiitic to alkalic basalts (MgO = 4.88–13.4 and SiO_2 = 43.4–50.0; Table 1 and Figure 4), with total alkali ($Na_2O + K_2O$) contents ranging from 2.14 to 5.39 wt%. Given that we will compare the isotopic and trace element signatures of the samples to mantle sources, all trace element ratios are discussed relative to the primitive mantle (McDonough & Sun, 1995). To characterize melting and source characteristics, the seamounts are described by differences in middle to heavy and light to middle rare earth element ratios ($[Sm/Yb]_N$ and $[La/Sm]_N$, respectively). These are summarized along with their major element and isotopic characteristics by region below. For reference, individual samples and seamount averages, as well as the averages for the data within each region are tab-

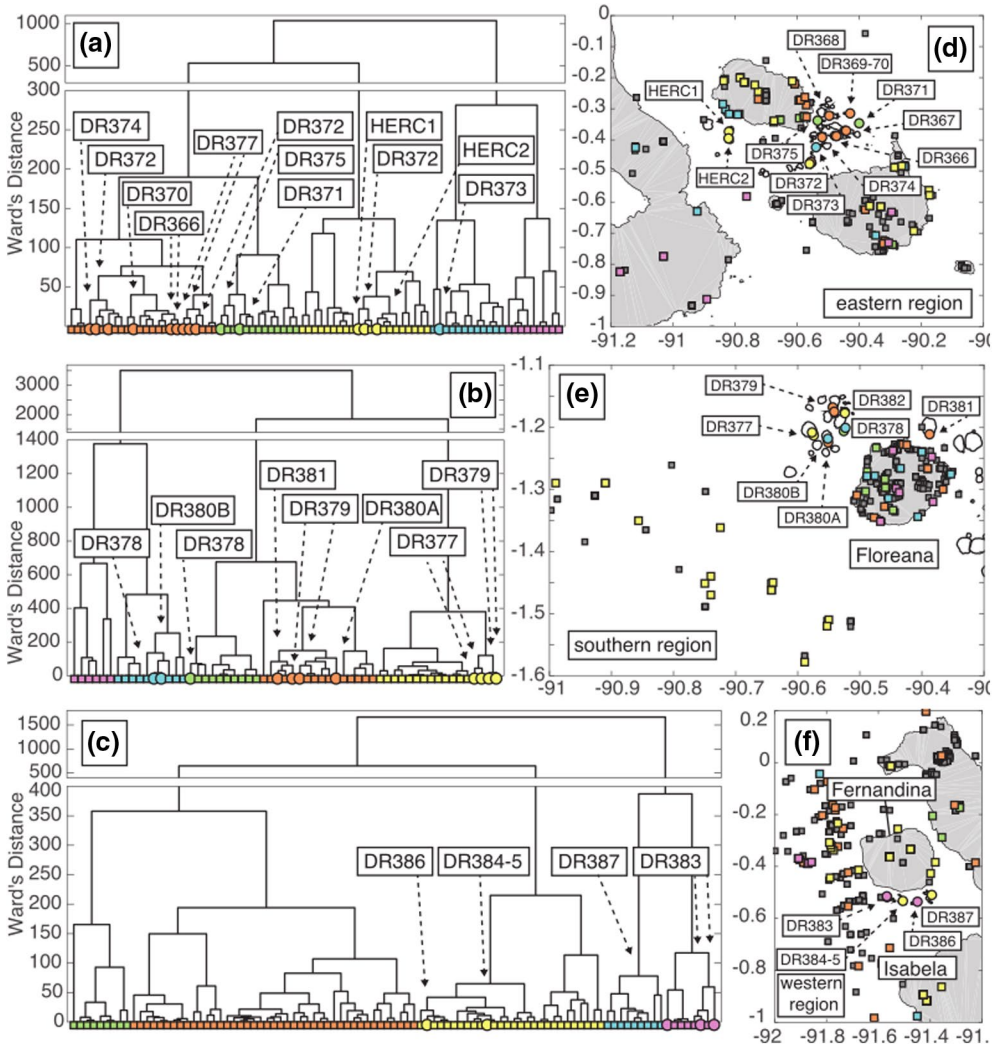

Figure 3. Dendrograms (a–c) and maps (d–f) for the eastern, southern and western seamount regions, compared to previous data. Note that the *y*-axis for plots (a–c) have been split into two scales to exaggerate details in early linkage steps. Sample symbology is the same as Figure 1. Filled colored boxes show the locations of panels in Figure 2. For each region colors and dendrograms show the results of the local agglomerative clustering analysis for all samples in each map region (see Section 3.5 for more details). The dive numbers for each seamount sample are given as labels in the dendrogram and map.

ulated in Table 1. Variable leaching experiments on isotopic measurements indicate that while Sr isotopic compositions are extensively affected by seawater contamination (Table S8), Nd is unaffected and is thus preferred in the interpretation of source variation between each seamount.

Clustering analyses compare the closeness of seamount sample compositions to other samples in the region. On the archipelago-wide scale, this comparison results in a dendrogram, where the final pair (at the top of the diagrams) separate clades of samples at a Ward's Distance of 5,493, or the greatest separation of trace element and isotope ratios between the two clades (Figure 1c). From top-to-bottom, branches connect clades of increasing similarity until each sample occupies its own branch (Figure 1d). Thus, samples connected at branches closer to the bottom of the diagram are more closely related in terms of geochemistry (Figure 1d). Five clades, that when separated result in the greatest reduction in Ward's Distance, are colored to visualize compositional affinities across the archipelago (Figure 1c). Results of the archipelago-wide and regional clustering analyses are shown in Figures 1 and 3. The archipelago-wide clustering analysis visually reproduces the broad domains observed by previous researchers, with three of the most prevalent affinities

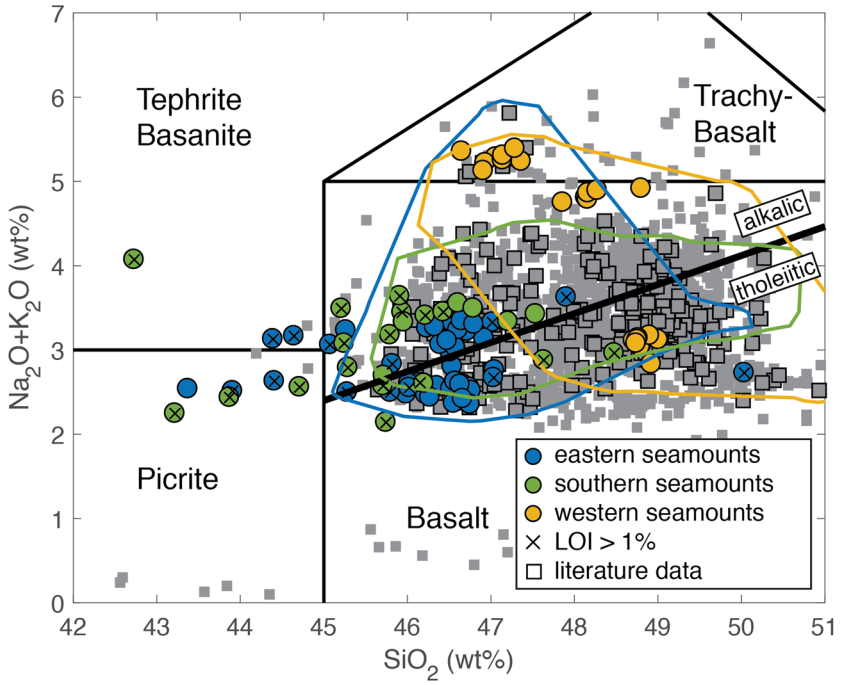

Figure 4. Total alkali contents as a function of silica for seamount samples compared to previously collected data. Seamount samples are shown as circles, colored by region. Samples with black X's had LOI >1%. Colored lines outline data used in the clustering analysis within each region, as defined by the extents of Figure 3 and shown in Figure 1 (see Section 3.5 for data references). Outlined gray squares are literature data used in the clustering analysis. Smaller gray squares show all other compiled literature data (see Table 1 for references). The division between alkalic and tholeiitic samples in the basalt field is from Macdonald and Katsura (1964).

represented in the east, south and west, with only a few samples represented by the remaining two affinities, located in the southern region (Figure 1a). In general, the seamount samples from this study fall within the variability previously observed in the archipelago (i.e., do not lie at the edges of the dendrogram). However, there are seamounts that have affinities not previously observed in individual geographic regions. This is particularly apparent in the southern region, where two seamounts (DR377 and DR382) are the only two features to have affinities (represented by pink and cyan) that are observed primarily in the northeast and the western regions (Figure 1a). The same is true, at least from a subaerial perspective, for the western region, where two seamounts have affinities that do not closely match those observed on the nearest island, Fernandina (DR383 and DR387). These archipelago-wide differences, which are only highlighted here, are described and evaluated in greater detail for each region in the following sections.

4.1. Eastern Region

Using the high-resolution bathymetry, 22 seamounts were identified in the eastern region (Schwartz et al., 2018a). Integrating the volume within the footprints of each of these mapped seamounts results in a total seamount volume of 6.4 km^3, which is 6% of the subaerial volume of Santiago Island (99 km^3). The average seamount volume is 0.07 km^3, which is the median of the three regions investigated here (Table 1). The eastern seamounts are spatially clumped into two primary regions, the first off of the southwestern flank of Santiago and the second between Santiago and Santa Cruz, off the east-southeast flank of Santiago (Figure 2a); however, we note that not all of the seafloor in this region has been mapped at a high resolution. The southeastern flank of Santiago harbors a majority of mapped seamounts (Figure 2a). The seamounts in this sub-region are variably elongate (mean aspect ratio = 1.7; Table 1) and form multiple lineaments parallel to the individual seamount elongations (mean elongation direction = 96°; Table 1). The elongation direction of the seamounts is similar to that of the elliptical island of Santiago (Figure 1) and the orientation

of its elongate volcanic vents (see Gibson et al., 2012). By comparison there are only two relatively conical seamounts in the southwestern region, as first described in Schwartz et al. (2018b). Generally, seamounts furthest from Santiago are the most conical, which includes the two seamounts on the southeastern flank of the island (Figure 2).

We analyzed 45 samples from 11 seamounts (and one from a lava flow front; DR373) southwest (NA-064; Schwartz et al., 2018b) and east-southeast (DR366-DR376) of Santiago. Together, the seamounts from both of these subregions are composed of relatively magnesian (MgO = 6.52–10.9; Table 1, Figure S2) tholeiitic to mildly alkaline ($K_2O + Na_2O$ = 2.35–3.34 wt%) basalts (Figure 4). Although the most alkalic samples are from the conical seamounts off the southwest coast of Santiago (NA-064), mildly alkalic samples are also observed in both the southwestern and eastern seamount subregions. In all cases these seamounts are low aspect ratio, conical vents, differing from the more elongate features directly to the east of Santiago (Figure 2a). Samples from each individual seamount have different trace element concentrations and ratios, resulting in a relatively wide range of compositions erupted in the region (e.g., $[La/Sm]_N$ = 0.757–1.59) (Figures 2 and 5a). However, all the samples erupted at an individual seamount are characterized by nearly uniform trace element ratios ($[La/Sm]_N$ < 4 % relative standard deviation [RSD]; Table 1), with the exception of one seamount, which spans nearly the entire range of chemical and isotopic variability observed in the region (DR372).

Isotope ratios for Santiago seamount samples from two linear-trends in bivariate isotope space (Figure 6). The two trends are pinned toward the more depleted isotopic endmember but diverge toward two more enriched compositions in Sr-Nd isotopic space (Figure 6). The eastern region seamounts have the most depleted compositions of all samples recovered and are more depleted compared to subaerial samples erupted on Santiago Island (Gibson et al., 2012; min. $^{87}Sr/^{86}Sr$ = 0.702639 and max. $^{143}Nd/^{144}Nd$ = 0.513085). Helium isotopic compositions for the eastern region seamounts are slightly greater than the average mid-ocean ridge basalt value of ~8.5 R/R_A and range from 8.49 to 10.4 R/R_A (Table 1). These values are between those of Santiago and nearby satellite islands, compositionally bracketed by Isla Daphne Major and Roca Bainbridge #3 (7.5–13.2; Geist et al., 2014a). Neither major or trace element contents directly correlate with isotopic enrichments of the seamounts, which is also true for He isotopes (Table 1).

In the clustering analyses, the eastern region seamounts are compared to lavas from adjacent islands of Santa Cruz, Santiago and part of Isabela (Figures 1, 3a, and 3d). Samples within the eastern region are separated at the highest linkage step with a total Ward's Distance of 1,039. None of the seamount lavas represent the most extreme values in the region (Figures 3c and 6). However, lavas fall within four of the five affinities in the region (Figure 3a), suggesting the seamounts are sampling significantly different melts. For seamounts with multiple samples in the clustering analysis, all except DR372 are linked on the first linkage step, meaning they are more similar to other lavas from the same seamount than to other seamounts or regionally analyzed samples. Thus, most seamounts are monogenetic. However, seamounts of different affinities are linked with other subaerial samples in the region earlier than being linked with other seamount samples. In other words, seamounts and subaerial samples do not form their own affinities. Only one submarine sample is separated from the other seamounts in the region at the greatest Wards Distance (DR373), suggesting it is the least similar to other seamount lavas. This sample was not actually collected from a seamount, but instead from edge of a large lava flow emanating from the northwest (Abbott & Richards, 2020) that may be related to Santiago. This sample is the most similar in composition to a few lavas erupted on the western edge of Santiago and to lavas erupted on Isabela and Santa Cruz.

4.2. Southern Region

A total of 61 seamounts were identified in the southern region (Schwartz et al., 2018a). The seamounts are located on the eastern, northern, and western flanks of the island of Floreana, but predominantly on the island's northeastern (Figure 2b) and western flanks (Schwartz et al., 2018a). The southern seamounts are the largest on average (0.09 km^3) and represent the greatest proportion relative to the adjacent subaerial volcano at 23% (seamount volume = 5.7 km^3; Floreana subaerial volume = 26 km^3). Of note, a previously unrecognized prominent northwest striking submarine volcanic rift zone emanating from Floreana island is observed in the new bathymetric data (Figure 2b). The rift is similar to, but smaller than, a rift emanating

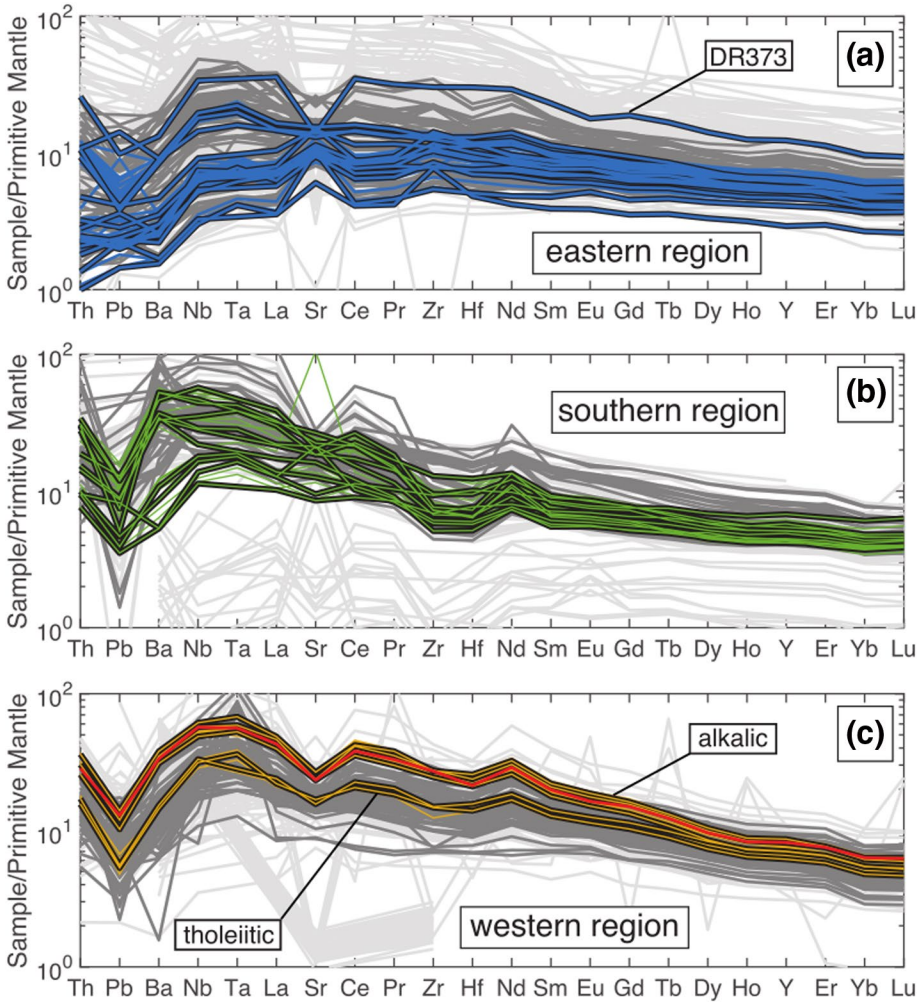

Figure 5. Spider diagrams showing trace element variability for each seamount region compared to representative data from each nearby island (a) eastern, (b) southern, and (c) western. Trace elements are ordered from most incompatible to least incompatible based on bulk partition coefficients for a basaltic melt from a peridotite (57% olivine, 13% clinopyroxene, 28% low Ca pyroxene, and 2% spinel). Partition coefficients for each mineral are averages of all values for each mineral from the Geochemical Earth Reference Model database (Table S10). Blue, green and gold colored lines are data from this study, as in Figure 4. Colored lines outlined in black are those with isotopes analyzed to show that isotopes were analyzed on the most extreme seamount samples and to highlight the differences in their trace element patterns, which are otherwise hard to distinguish. All other lines show literature data defined by the map extents in Figure 3 and are dark for those in the clustering analysis (see Section 3.5 for references) and light for all other data (see Table 1 for references). Red line in (c) shows average deep water lava flow (DWF) sampled in situ at the leading edge of the Galápagos platform (Anderson et al., 2018).

from the island's southwest flank, which has been likened to other rift zones that are observed on the western islands (Harpp et al., 2014b).

We measured 28 lavas from seven seamounts west of Floreana (no samples were collected east of Floreana). Similar to the eastern region seamounts, the composition of samples from individual seamounts are generally more homogenous than the seamount region as a whole ($[La/Sm]_N$ = 1.4–4.7 for all seamounts; Figures 2 and 6; $[La/Sm]_N$ < 5 %RSD for five out of six seamounts; Table 1). Southern region seamount samples are distinguished from the other Galápagos seamount lavas by concave-up light Rare Earth Element patterns (Figure S3). All southern region seamount samples form a linear, albeit scattered array in Nd-Sr isotope space (Figure 6). Floreana samples are characterized by radiogenic Sr compositions (e.g., average. $^{87}Sr/^{86}Sr$ = 0.70340), with intermediate $^{143}Nd/^{144}Nd$ (0.51296) (Table 1). Similar to the eastern region, there

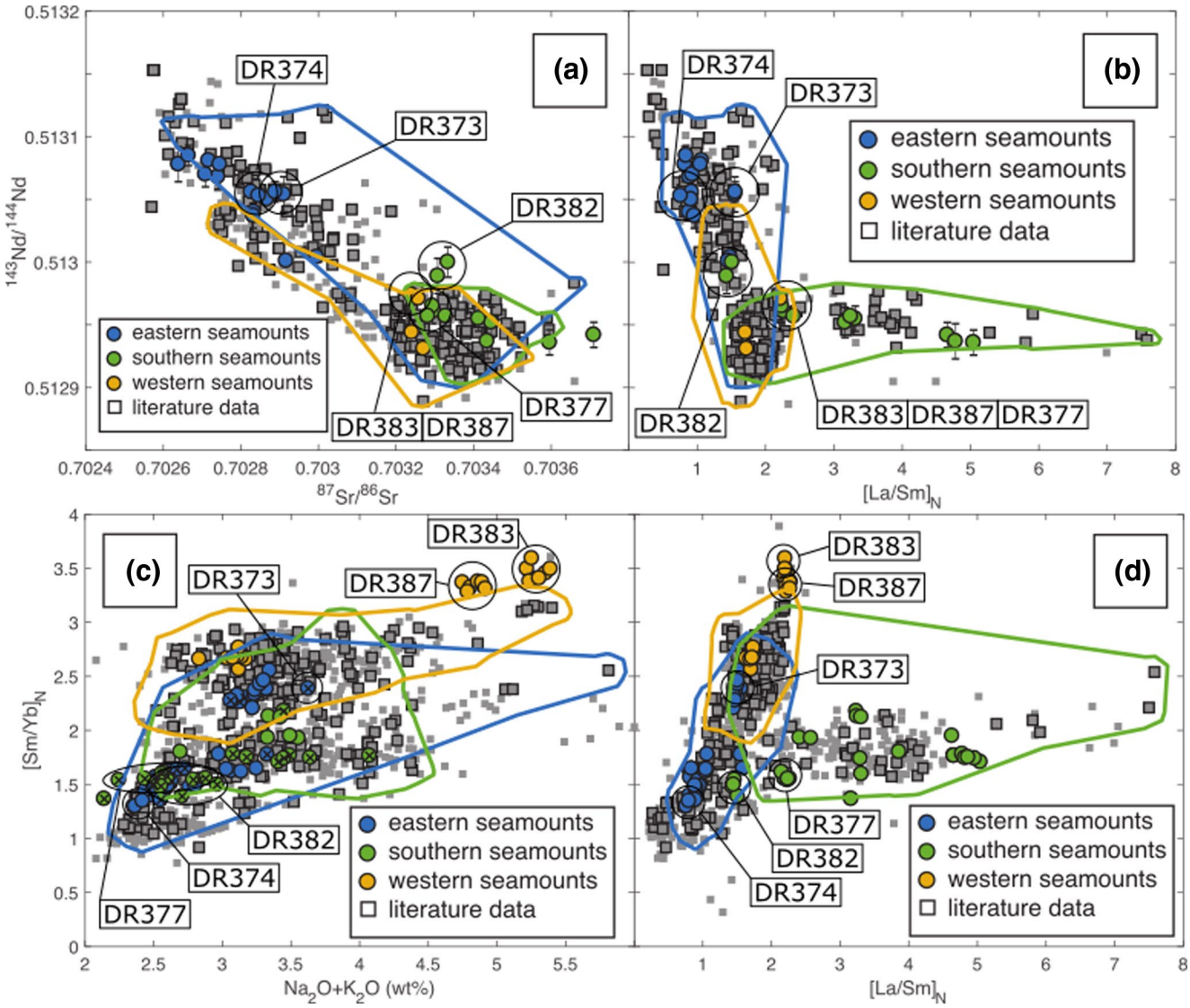

Figure 6. Trace element and Isotopic variation of seamounts compared to previously published data. Seamount samples are shown as colored circles. Colored lines outline data used in the clustering analysis within each region, as defined by the extents of Figure 3 and shown in Figure 1. Gray outlined squares are literature data used in the clustering (see Section 3.5 for references). Smaller gray squares show all other compiled literature data (see Table 1 for references).

are no clear trends in major and trace element data with seamount morphology or geography (Table 1 and Figure 2).

We compare southern region seamounts to samples from Floreana island and submarine platform samples to the southwest of the seamount sampling area (Figures 1 and 3e). Samples within the southern region are separated at the highest linkage step with a total Ward's Distance of 3,506. This value is more than twice that of the eastern and western regions, despite including the fewest samples (Figure 3), highlighting the extreme variation observed in the south of the Galápagos. Similar to samples previously analyzed on Floreana Island (e.g., Harpp et al., 2014b), seamount lavas show nonsystematic isotopic and trace element enrichment patterns, geographically (e.g., $[La/Sm]_N$; Figures 2 and 6). The seamount lavas have compositions similar to the range observed on Floreana Island (Figure 5). However, two seamounts have isotopic ratios that more closely resemble eastern and western region samples, than anything else yet observed in the area (DR377, DR382; Figure 6). These are most similar to regional lavas dredged from the edge of the Galápagos Platform, southwest of the island. This difference is highlighted in the regional agglomerative

clustering analysis, where these two seamounts are the only ones in the southern region that have affinities predominantly observed in the west and east and represent an endmember for the region (Figures 1a and 1c). These samples have less enriched isotopic signatures and are similar to the most isotopically enriched samples at Santiago (Gibson et al., 2012). Interestingly, unlike the eastern seamounts, lavas from these two southern seamounts still have concave-up Rare Earth Element patterns (Figure S3), but less pronounced enrichment in fluid mobile trace elements like Ba, and higher Hf relative to Nd (Figure 5). The southern region seamount lavas have intermediate $^{3}He/^{4}He$, between 12.4 and 15.1 R/R_A. These values expand the upper and lower bounds of previous Floreana measurements (13.4–14.4; Kurz & Geist, 1999) and do not directly correlate with other isotopic ratios (Table 1).

4.3. Western Region

Using bathymetric data, 18 seamounts were identified in the western region, all of which were mapped on Fernandina's southern flank (Schwartz et al., 2018a). Unlike the other study areas, these seamounts do not sit on top of the volcanic platform but are situated on the submarine flanks of Fernandina. The seamounts have an average volume of 0.06 km^3, which is the smallest of the three regions (Table 1). Correspondingly, the total mapped seamounts volume (1.2 km^3) accounts for the lowest absolute volume and lowest percentage of the subaerial island volume of Fernandina (<1%), which is 191 km^3. In total, the seamount volume is on the order of what is estimated for single subaerial eruptions on Fernandina (1–2 km^3; Simkin & Howard; 1970). Seamounts morphologies are either conical (e.g., DR383 and DR387), or are elongate features comprising either stair stepping flat top cones (e.g., Clague et al., 2000) or a sharp ridge oriented radially to Fernandina's summit (e.g., DR386) (Figure 2c).

We analyzed 22 samples from four seamounts south of Fernandina (Figure 2c). Unlike the previously described seamount regions, these samples from two distinct, chemical domains (mildly alkalic, DR383, DR387 and tholeiitic DR384–5 and DR386; Figure 4 and Table 1), and show limited chemical variation within each cluster (%RSD of $[La/Sm]_N$ <2%; Table 1). These domains are distinct in major elements (Figure 4) and trace element ratios (e.g., high total-alkali samples have higher trace element contents; Figure 5 and higher $[La/Sm]_N$; Figure 6a). Tholeiitic seamount lavas have compositions most similar to subaerial Fernandina and form the elongate volcanic features (northwest-southeast trending fissure and the northwest-southeast trending series of flat-topped stepped seamounts) (Table 1 and Figure 2). By contrast, the more alkalic lavas produced the circular, point source seamounts and are unlike any subaerial Fernandina lavas, but are chemically similar to two deep water (~4,000 m) alkalic lava flows located on the seafloor at the western leading edge of the Galápagos Platform (Anderson et al., 2018, Figure 5). Western region lavas are intermediate in Sr isotopes ($^{87}Sr/^{86}Sr = 0.703239–0.703271$; Figure 6) but with the least radiogenic $^{143}Nd/^{144}Nd$ (0.512931; Figure 6) and the highest $^{3}He/^{4}He$ of 23 R/R_A (Table 1). Notably, lavas from seamounts in the western region show very little variation in Sr isotope ratios, with variation in Nd isotopes, which is different than the other seamount region mixing arrays. Nd isotopes negatively correlate with trace element enrichment, where alkalic lavas have enriched isotopic compositions (Figure 6a).

In the western region, the seamounts are compared to samples from the adjacent islands of Fernandina, Isabela, and the submarine platform (Figures 1, 3a, and 3d). Samples within the western region are separated at the highest linkage step with a total Ward's Distance of 1,663. Alkalic samples have most extreme $(Sm/Yb)_N$ (Figure 6c). The two seamounts with tholeiitic compositions are indistinguishable from those erupted on subaerially Fernandina, or samples with that affinity (Figure 3f). The alkalic samples are classified in the same affinity as those from deep water flows at the western extent of submarine sampling (Anderson et al., 2018, Figure 3c). The two seamounts are indistinguishable from these deep water flow samples, in that they are not next to each other at the lowest levels of the classification (Figure 3c). However, the deep water flow lavas and these two alkalic seamounts are the only two lavas of that affinity.

5. Discussion

5.1. Seamount Heterogeneity and Relation to Surrounding Islands

Our bathymetric data show that seamounts constitute a smaller, yet significant volume of material relative to the subaerial islands (Table 1), although both are dwarfed by the volume of the volcanic platform. In general, the seamounts appear to be primarily monogenetic in their construction. For example, lavas erupted at individual seamounts have limited variation in major element contents and trace element ratios (e.g., %RSD of $(La/Sm)_N$ is < 4% at 17 of the 18 seamounts where there are at least three analyzed samples; Table 1). This observation is supported by results of the clustering analyses, where lavas from individual seamounts are clustered in the first linkage steps, indicating similarity in composition (Figures 1c, 1d and 3). This suggests that each seamount formed from a single or a series of closely timed eruptions from a single batch of magma. One exception is DR372, which has three samples that are not linked in early steps of the clustering analysis and are separated into three different affinities, suggesting the eruption of distinct magma batches (Figure 3a).

Based on variability in isotopic (Figure 6b) and trace element ratios that are invariant to fractionation for small degrees of crystallization (e.g., $[La/Sm]_N$; Figure 6b), it is clear that the seamount fields as a whole (eastern region, southern region, and western region) must have formed through multiple episodes of volcanism sourced from different magma batches. For example, in the eastern region samples from DR375 ($[La/Sm]_N = 1.05$) must be produced by a melting event or mantle source that is different to that of seamount DR374 ($[La/Sm]_N = 0.77$) despite their geographical proximity (Figures 2a and Table 1). This is further supported by the clustering analyses, where samples from these two seamounts are not linked in early steps and are separated into different regional affinities (Figures 3a and 3d). Similarly, seamounts in the southern region show much less variability at individual seamounts in comparison to the seamount region as a whole (Table 1 and Figures 1–3) and samples from different seamounts fall into different affinities on the regional scale (Figures 3b and 3e). Seamounts in the western region show the least intra-seamount variability of the three regions (RSD of $[La/Sm]_N$ <2%; Table 1). However, unlike other regions, the western seamounts form two groups based on geochemistry and morphology (Figures 2 and 3c), including an alkalic and tholeiitic group (Figure 4) and have separate affinities in the clustering analysis (Figure 3c). Of note, the samples from the alkalic seamounts are within an affinity not observed on Fernandina Island and previously only observed at the western submarine extent of sampling (Figure 3f). We note that although there are alkalic and tholeiitic seamounts in the Santiago region, they are not as distinctly clustered (Figures 1c and 3a).

At monogenetic volcanic fields, magma is either focused through the volcano's central magmatic plumbing system and then redirected via lateral dikes (e.g., Muirhead et al., 2016; Walker, 2000) or emplaced through the vertical ascent of magmas that bypass the magmatic plumbing system of the central edifice (e.g., Needham et al., 2011). In the former case, there may be little variability in the compositions of the submarine and subaerial samples as magmas are mixed within the shallow system prior to eruption. In the latter case, there may be significant chemical variations among monogenetic volcanoes themselves that may provide insights into the length scale and structural heterogeneity in the mantle or small-scale variations in melting systematics (e.g., LeCorvec et al., 2013; Rasoazanamparany et al., 2015). In the following sections, we evaluate the origins of the geochemical heterogeneity of each seamount region relative to the adjacent islands to determine if the seamount lavas are sourced from the central magmatic system and then summarize the results on the archipelago scale.

5.1.1. Eastern Region

Samples erupted on the island of Santiago previously have been divided into two spatially and geochemically distinct lavas (Gibson et al., 2012; Swanson et al., 1974). The island contains alkalic and isotopically enriched basaltic samples in the west and tholeiitic, isotopically depleted basalts to the east. However, enriched and depleted samples are not strictly isolated to these two sub-regions and are interpreted to have been erupted coevally (Gibson et al., 2012), which makes it unique for a Galápagos volcano. Thus, these variations are not interpreted to arise as a result of an evolutionary sequence of the island (Swanson

et al., 1974). Based on this, and geophysical evidence for lithospheric thickness variations between the west and east across Santiago (Villagomez et al., 2007), it has been suggested the difference in chemical composition of erupted samples to the east and west of this divide results from a change in the total extents of mantle melting (Gibson & Geist, 2010; Gibson et al., 2012). In this model, samples erupted in the east are produced by higher extents of melting, while samples erupted in the west result from lower extents of melting. However, Gibson et al. (2012) note that trace element enrichment cannot be entirely attributed to variations in melting, given that samples on each side that have similar trace element contents can have different isotopic ratios. Nevertheless, the preservation of two spatially and geochemically distinct magma types, with differing source characteristics, suggests that the melts are not homogenized in a single, centralized shallow magma reservoir prior to eruption (Gibson et al., 2012). Instead variations result from vertical ascent of melts, with different source characteristics resulting from lower degrees of melting in the west compared to the east (Gibson et al., 2012).

The seamounts in the eastern region generally conform to the broad spatial chemical division of Santiago, where the most alkalic lavas were erupted at the western seamounts and the more tholeiitic samples erupted in the east (Figure 2a). Tholeiitic samples in the eastern seamount province have the same depleted trace element patterns as the island tholeiites (Figure 5a). Similarly, a detailed investigation of samples erupted at the two western-seamounts shows they are nearly compositionally identical to a subset of subaerially erupted alkalic lavas, suggesting that the magmas were transported laterally from the western magmatic center onto the submarine flanks (Schwartz et al., 2018b). Furthermore, many of the seamounts in the east have elongate or linear vents that are oriented radially from Santiago and aligned with its subaerial vent structures (Figures 2 and 3; Gibson et al., 2012; Swanson et al., 1974), suggesting that the seamounts may be an extension of the subaerial magmatic system. Combined, these observations indicate that the seamount samples in this region may pass through one of Santiago's centralized plumbing systems prior to being redistributed out toward its flanks onto the seafloor via lateral diking.

Despite apparent processing through central magmatic systems, the seamount samples are more mafic on average than samples erupted on Santiago, meaning that seamount lavas are likely a closer representation to primary magmas than those erupted on the subaerial portion of Santiago. This observation aligns with interpretations of submarine flank volcanism in Hawai'i (Garcia et al., 1995) and the submarine flanks of Fernandina (Geist et al., 2006), where picritic lavas, sampled only in dredge-recovered submarine glasses are interpreted to result from the lateral emplacement of these lavas from deeper portions of the island's magmatic systems. Furthermore, we note the difference in composition between the sample collected from the submarine lava flow emanating from SE Santiago (DR373), compared to the rest of the seamount samples. DR373 is more evolved and has a composition most similar to Isabela and Santa Cruz. The evolved characteristics of this lava flow are more indicative of a lava that was erupted from a magma that evolved in a shallow magma reservoir (Naumann & Geist, 2002) than that of the seamount lavas. This observation, and the absence of seamount lavas of similar compositional characteristics, could indicate that it was formed from a more robust phase of volcanism at some point in the volcano's history.

5.1.2. Southern Region

Floreana volcano, at the southern extent of the archipelago, erupts lavas that are geochemically distinct in both trace element patterns and radiogenic isotope ratios compared to all other Galápagos islands (Harpp & White 2001; Harpp et al., 2014b; White et al., 1993). The samples are typified by high concentrations of fluid mobile trace elements (e.g., elevated $[Ba/La]_N$), have concave-up normalized trace element patterns, and the most radiogenic Sr and Pb isotope compositions (Harpp et al., 2014b). Based on the extreme variability of subaerial samples it is hypothesized that there is no centralized magma chamber at Floreana to homogenize melts prior to eruption (Harpp et al., 2014b). Despite the island's unique chemistry, studies of cumulates erupted in subaerial lavas provide evidence for evolution from a Fernandina-like source (Lyons et al., 2007). This is interpreted as evidence that the mantle source feeding eruptions on Floreana has transitioned from more PLUME to FLO as the island has migrated over the center of plume upwelling (Harpp et al., 2014b). However, similar compositions to PLUME-like samples have not been observed in subaerial lavas, perhaps because they have been buried by subsequent eruptions.

There is a wide range of $(La/Sm)_N$ observed in all of the southern region seamounts (Table 1), which form a random geographic distribution (Figure 2). This observation supports the hypothesis that most lavas are not erupted from a single steady-state magma reservoir, which would presumably homogenize samples prior to eruption (Harpp et al., 2014b). However, the identification of a submarine rift zone emanating radially from the northwest flank of Floreana, suggests that the island may have supported a centralized magma reservoir in its past and therefore was once more magmatically active than currently represented on the subaerial island.

Trace element and isotopic data show that the southern region seamounts generally have the most incompatible trace-element enriched signatures of all the seamount samples (Figure 6), such as elevated $(Ba/La)_N$ (Figure 5) and the characteristic concave-up trace element patterns (Figure S3), typifying the FLO mantle endmember (Harpp et al., 2014b). However, the seamounts in this region expand on the heterogeneity previously observed in subaerial lavas in the region (Figures 1a, 1c, 5b, and 6). In particular, two seamounts (DR377 and DR382) have lower Sr isotopic compositions (Figure 6b), $(La/Sm)_N$ (Figures 2b and 6a) and $(Ba/La)_N$ that are more similar to those of eastern and western regions (Figure 5). This difference is exemplified in the in the regional clustering analyses, where these two seamounts form a clade within themselves that lies at the edge of its affinity (Figure 3b). In the archipelago-wide clustering analysis (Figure 1a), samples from DR377 are classified to have the same affinity as the platform samples in the region, which typifies the affinity in the western region in the archipelago (i.e., PLUME). Thus, the samples from DR377 seamounts provide complementary evidence that southern region magmatism is sourced from melts derived from variable proportions of multiple source components, like those of the western volcanoes during its evolution (Lyons et al., 2007). Additionally, samples from DR382 more closely resemble the affinity of those in the eastern region (i.e., DUM) (Figures 1a and 1c), further supporting the heterogeneous nature of the southern seamounts.

5.1.3. Western Region

Subaerial Fernandina erupts some of the most monotonic tholeiitic samples in the modern Galápagos Archipelago (Allan & Simkin, 2000; Geist et al., 2014b; Saal et al., 2007). This suggests that lavas are compositionally buffered by a steady state magma reservoir (Geist et al., 2014a). These inferences are corroborated by interferometric synthetic aperture radar measurements of volcano inflation and deflation, which confirm the presence of a shallow magma reservoir (Bagnardi & Amelung, 2012). This shallow centralized magmatic system appears to be directly connected to radial and circumferential vents on the volcano (Bagnardi et al., 2013; Chadwick et al., 2011). Radial vents on the western Galápagos volcanoes, in particular, provide evidence that magmas routinely undergo lateral transport from the volcano's center to its flanks.

Although subaerial lavas have a clear connection to the centralized magmatic system, the seamounts erupt both tholeiitic and alkalic compositions, suggesting a more complex system. The tholeiitic seamount lavas have major, trace element, and isotopic compositions that closely resemble subaerially erupted Fernandina samples (Figures 4–6). Furthermore, the tholeiitic seamount samples are all erupted from ~northwest-southeast oriented vents that generally align with the trend of the subaerial vents. The similarity in vent orientation and chemistry of the submarine and subaerial samples suggests that the tholeiitic seamounts are the submarine extension of the same volcanic plumbing system that sources radial vents subaerially.

By contrast, the alkalic seamounts are conical, and appear to be point source volcanic features (Figure 2c). They have higher incompatible trace element abundances (Figure 5) and more steeply sloped primitive-mantle normalized trace-element and Rare Earth Element patterns than the tholeiitic samples from the region (Figure S3). Additionally, the alkalic seamount samples have slightly more radiogenic Nd isotopic compositions for a given Sr isotopic compositions (Figure 6a). There are also no known subaerial alkalic samples erupted on Fernandina. Combined, this suggests that the alkalic magmas bypass Fernandina's present-day shallow magma reservoir. Instead, the seamount alkalic samples are compositionally identical to alkalic deep water lava flows sampled in situ on the seafloor at the leading edge of the Galápagos plume (Figure 5c; Anderson et al., 2018) and similar, but more alkalic than, those sampled to the north at Roca Redonda (Standish et al., 1998).

5.1.4. Archipelago-Wide Summary

The diversity of seamount samples in each region indicate both a connection to and isolation from the magmatic systems of the subaerial volcanoes. In some cases, seamount samples can be directly linked to subaerially erupted samples (Figure 5), suggesting that they are processed through the central edifice of the volcano. This is particularly evident in two seamounts at the western edge of the eastern seamount region (Schwartz et al., 2018a), and a subset of western seamounts compared to Fernandina (tholeiitic group; Figures 4–6), where seamount lavas are nearly indistinguishable from subaerially erupted products (Figure 3c). However, there is more chemical diversity recorded in the seamounts at both Fernandina and Floreana compared to the islands that they surround (Figures 1 and 6) despite fewer samples, suggesting that seamounts can record more unique magmatic events than what is preserved on the islands. These contrasting observations are similar to submarine sampling in Hawai'i (Cousens & Clague, 2015; Greene et al., 2010), which is the only other archipelago that has been sampled in similar detail. In Hawai'i, seamounts often fall within geochemical fields of the nearby islands however, in both studies, some seamount samples expand upon what is observed.

The above observations suggest that while the islands have been at least partially repaved by ongoing volcanism, or, in the case of the western volcanoes, all the exposed magmas are being homogenized within a central system, the seamounts may preserve the complexity of chemical variations in some regions of the Galápagos Archipelago and elsewhere. Thus, seamount lavas may bypass the island centralized magmatic systems and retain more primitive compositions or be preserved by a lack of repaving and provide new insights into ocean island evolution.

No additional geochemical variability of seamounts compared to the volcanic islands is observed in the eastern archipelago. Therefore, we suggest that the lack of a centralized vent system may be a persistent feature of these volcanoes. As a result, the significance of a selection bias, related to sampling large edifices, is reduced. Conversely, for more magmatically active volcanoes, which have established centralized vent systems, this bias is accentuated. Nevertheless, the observation of only sparse samples that fall outside of previously observed heterogeneity, highlight the importance of targeting large numbers of features (e.g., seamounts) when testing ocean-island evolution and plume heterogeneity models in detail. Furthermore, even though samples from the eastern region do not expand the heterogeneity previously observed in the region, the fact that they are more mafic on average than what has been sampled subaerially means that submarine sampling may provide a means to recover rocks which most closely represent primary mantle melts.

5.2. Seamount Insights Into Ocean Island Evolution

Plume theory predicts that ocean islands evolve systematically as a function of proximity to the plume center, which is primarily modulated by plate motion (Morgan, 1971). Hawai'i serves as the type example for ocean island evolution as it relates to plume theory, where islands undergo a series of evolutionary phases related to increasing and decreasing magma flux controlled by the relative position of islands and hotspot source (Clague & Sherrod, 2014). This progression begins with a low magma supply alkalic stage at the leading edge of the plume (typified by Lō'ihi; Moore & Clague, 1982), but also observed west of Mauna Loa, in submarine radial vent lavas (Wanless et al., 2006b). As the plate moves over the plume center, the volcano transitions into a shield building, tholeiitic main stage (Clague & Sherrod, 2014) and then back to an alkalic post-shield building phase as it passes beyond the center of upwelling. The volcano may undergo a later rejuvenated highly alkalic phase related to a second stage of decompression melting at the periphery of a hotspot swell (Bianco et al., 2005). While this evolution has been well documented in some ocean island systems (Albarède et al., 1997; Carracedo, 1999; Devey et al., 2003), it is less obvious at other archipelagos, including the Galápagos (Harpp & Geist, 2018). We hypothesize that some inconsistencies between the Galápagos and traditional plume theory can, in part, be explained by a sampling bias compared to Hawai'i where more of the small-scale volcanism has been sampled in detail (Cousens & Clague, 2015; Greene et al., 2010; Moore & Clague, 1982; Wanless et al., 2006a, 2006b).

A recent study of deep water flows collected in situ from the seafloor west of the Galápagos platform reveal the presence of alkalic lava flows at the leading edge of the plume (Anderson et al., 2018). Based on geo-

chemical analyses and numerical models, these lavas are interpreted to be the result of lower degree melts produced during the early stages of melting of the Galápagos plume. The alkalic Fernandina samples were collected from seamounts on the submarine flanks of the volcano and have nearly identical geochemical characteristics to the deep water flows (Figure 5c), thus they were likely formed from a similar process. Therefore, for a detailed discussion into the origins of these alkalic lavas, the reader is directed to Anderson et al. (2018). In summary, the trace element enrichment of the alkalic samples is accompanied by extreme enrichments in middle-to-heavy Rare Earth Element ratios (e.g., high $[Sm/Yb]_N$; Figures 6b and 6c), and very little isotopic variation, compared to tholeiitic samples from the same region (Figure 6a). The decoupled behavior of $(Sm/Yb)_N$ and isotopic ratios is inconsistent with origins related to variations is the mantle source (e.g., Gibson et al., 2012). Alternatively, the enrichment of $(Sm/Yb)_N$ is predicted for melts originating in the presence of garnet, due to a 10-fold difference in compatibility of HREEs compared to MREEs in garnet (Table S10). Although variable $(Sm/Yb)_N$ enrichments are observed in samples throughout the archipelago (White et al., 1993), the extent of enrichment depends on the relative proportion of melting occurring in the garnet stability field, modulated by the depth of melt initiation and the truncation of melting (Gibson & Geist, 2010). Thus, the higher $(Sm/Yb)_N$ of the alkalic compared to tholeiitic lavas in the western region support that they are derived from a greater proportion of melting in the presence of garnet (i.e., at greater mean depths). We suggest that the onset of volcanism at the leading edge of the archipelago in the Galápagos likely consists of alkalic magmas resulting from low-degree melts, similar to observations of geochemical evolution of ocean islands in Hawai'i (Clague et al., 2014) and is a consequence of progressive melting of a fixed hotspot source predicted by plume theory (Watson & McKenzie, 1991; Campbell, 2007).

The only difference between the seamount alkalic seamounts and the alkalic deep water flows is that the former are located on the shallower flanks of Fernandina volcano (Figure 2). The presence of alkalic samples higher up in the volcanic stratigraphy in Fernandina confirms that the eruption of low degree melts is a modern part of the growth of Galápagos volcanoes. The observation of submarine alkalic samples on the leading island's flanks is somewhat analogous to Hawai'i, where submarine sampling at Lō'ihi was required in order to observe the same phenomenon (Moore et al., 1982). However, the scale of the submarine feature that records this progression is much smaller in the Galápagos, hence it has been previously missed from sampling. To date, a similar systematic decrease in the extent of melting as the islands migrate away from the plume center in has not been observed in the Galápagos. This may result from the majority of sampling being restricted to the younger portion of the archipelago. Alternatively, it could reflect inherent differences in the Galápagos and Hawai'i systems (Harpp & Geist, 2018). However, the observation of an evolved Isabela-like submarine lava flow in the eastern region, and a submarine rift zone in Floreana may provide evidence that these volcanoes have experienced a higher-volume phase of volcanism in their pasts. Better age control on these submarine samples would likely resolve this relationship in terms of ocean-island evolution.

5.3. Seamount Insights Into Mantle Plume Zonation

Conventional "plume theory" makes no explicit predictions about mantle composition but OIBs show the most extreme compositional variation of all ocean basin lavas and are often used to investigate mantle heterogeneity owing to their deep mantle origins (e.g., Hofmann, 1997). Chemical variations in OIBs reflect a combinaFisktion of shallow and deep magmatic processes, while, isotopic variations are thought to reflect longstanding heterogeneities in the mantle from which they are sourced (Hart et al., 1992; Hofmann, 1997). Differences in the isotope composition of individual islands are often interpreted to represent the length scales and relative distributions of deeply seated mantle source reservoirs. For instance, longstanding temporal variations in lavas erupted at single ocean island chains have resulted in schematic illustrations of the mantle, where reservoirs are simplified into distinct domains, hundreds of kilometers in scale (Hawai'i; e.g., Abouchami et al., 2005; Galápagos; e.g., Gazel et al., 2018; Hoernle et al., 2000). Geographic isotopic patterns within and between ocean islands are explained by the variable tapping of these numerous reservoirs (Hart et al., 1992), each sequestered somewhere in the mantle (Castillo, 1988; Hoernle et al., 2015; Hofmann, 1997; Harpp et al., 2014a; Mazza et al., 2019; Weis et al., 2011). Alternative models suggest that the mantle is heterogeneous on short length scales and persistent geographic patterns in isotopic signatures in the ocean island record are only apparent given the nature of mantle melting at ocean islands themselves (Bianco et al., 2011, 2008 and; Ito & Bianco, 2014; Jones et al., 2016, 2017).

Although there is little consensus on the length-scale and geometry of isotopic endmembers in the Galápagos, a dominant interpretation of the geographic pattern of geochemical variability is that it is the result of melting of large-scale mantle domains (Harpp & White, 2001; White et al., 1993), which have persisted in the same configuration for much of the hotspot's history (Gazel et al., 2018; Geldmacher et al., 2003; Hoernle et al., 2000). These domains have isotopic compositions that are less extreme than the principle components identified by Harpp and White (2001). This observation is interpreted to represent mixing of the source endmembers, prior to eruption in each of the domains (Harpp & White, 2001). If this is the case, one prediction of a predominantly island-based sampling bias is that samples from small seamounts, which bypass mixing on the island scale, could have isotopic compositions that more closely match the extreme values of the principle components. This is not observed in our dataset, where all of the seamounts have compositions that fall within the isotopic range of previous samples. Nevertheless, higher resolution sampling can be used to investigate whether or not the apparent domains are a mixture of different proportions the mantle endmembers identified through the principle component analysis of Harpp and White (2001), and how many (between one and three) components are involved in this mixing. We cannot assess whether all four principle components of Harpp and White (2001) are mixing in each region and their relative proportions without Pb isotopes, due to the fact that the WDL component is distinguished from that of DUM by anomalously high $^{208}Pb/^{204}Pb$ (Harpp & White, 2001).

If the domain model does not represent variable mixing between all principle components, we would expect seamounts to be dominated by the local domain composition assuming they are co-genetic with the island or an upstream domain if they are older. In general, we observe that the monogenetic seamounts generally have geochemical characteristics similar to those of the islands that they surround, supporting a domain concept (Figures 5 and 6). However, some Santiago and Floreana seamounts are geochemically distinct from one another (Figures 1, 3, and 6). For these regions, mixing must occur between at least three distinct geochemical endmembers in order to produce the complex spread in isotopic data (Figure 6b). Although this is observed sub-aerially in the eastern region (e.g., Gibson et al., 2012), this was not previously clear for Floreana in the south. Southern region seamount lavas clearly have compositional characteristics aligning closely with PLUME, DUM/WDL, and FLO affinities (Figure 1). Neither the DUM or WDL affinities are predicted to be involved in the southern domain if it does not represent mixing of all principle components and these domains are oriented in the mantle with PLUME in the west, DUM in the east and FLO to the south (Hoernle et al., 2000). This suggests that domains are, instead, a manifestation of variable mixing between multiple mantle endmembers in each region.

Within a given region enriched and depleted seamounts are scattered at random suggesting short-scale heterogeneities (Figure 2). In order to tap these heterogeneities in such proximity (different isotopic composition of seamounts <1 km apart; Figure 2), the length scales of the isotopic domains in the mantle must be on or less than that scale, supporting the short scale heterogeneity models of Gibson et al. (2012) and Harpp et al. (2014b), as opposed to large-scale mantle endmembers (>100 km zones; e.g., Hoernle et al., 2000). As an alternative to large geochemical zonation in the mantle, it is possible that consistent broad patterns of geochemical heterogeneity can be brought about through melting systematics of various lithologies (e.g., Jones et al., 2017).

6. Conclusions

We have sampled small near-island seamounts from three sub-regions of the Galápagos Archipelago and compared their geochemical characteristics to literature data to evaluate the significance of a potential selection bias associated to sampling of primarily large subaerial volcanic edifices. This study shows that almost all individual seamounts sampled are chemically homogeneous, when compared to the overall variation in chemistry between seamounts within any given region. This similarity in composition suggests that most seamounts are monogenetic and erupted during the same magmatic event or under similar magmatic conditions. This observation indicates that these small volcanic constructs are likely good targets for evaluating magmatic processes through time, in that they are not repaved through multigenetic eruptions, as are large edifices. This is true even if only limited sample is collected from individual seamounts, which is typically the case for submarine sampling campaigns.

Variations in major, incompatible trace element and particularly isotope ratios between seamounts in each region result from magmas produced from slightly different mixtures of the three primary Galápagos mantle endmembers, as well as variations in extents of melting. This suggests that although seamounts are generally generated from discrete magmatic events, they collectively represent a range of processes/events that produce their geochemical diversity. Some seamounts have samples that appear identical to subaerially erupted samples, while others do not. Nevertheless, there is more chemical diversity erupted at the seamounts compared to the islands, suggesting that some seamount samples bypass mixing in the main magmatic system or that the seamounts preserve more unique magmatic signatures than large volcanic edifices sampled in the past. This means that seamounts can provide a wider window into mantle processes compared to samples erupted on the islands themselves. However, we note that seamount construction as a byproduct of ocean-island formation, necessitates that a large number of features need to be sampled, in order to capture these nuances. Moreover, some ocean islands may be more susceptible to a selection bias than others. In particular, islands that do not show evidence for a centralized magmatic system may not be as affected as ones that do, given that magmas are not being as readily homogenized prior to eruption. However, in cases where volcanoes do not show evidence for a centralized magmatic system in the Galápagos today, submarine observations and sampling may recover samples that more closely resemble primary mantle melts than their subaerial counterparts (which is true for the eastern seamount region) or evidence that shallow magma chambers were once supported in the past, as exemplified in evolved samples recovered in the eastern sampling region and identification of a submarine rift system surrounding Floreana in the south.

Incompatible trace element and isotopic characteristics of seamounts are used to evaluate the source contributions to the seamount samples. Seamounts with alkalic compositions on the flank of Fernandina in the western region of the Galápagos are indicative of low-degree melting at the leading edge of the Galápagos hotspot, which are not observed subaerially. We suggest that these seamounts represent low-volume melts, associated with incipient melting at the leading edge of the Galápagos plume. We believe these samples are akin to the pre-shield phase of volcanism observed at Lōʻihi in Hawai'i, as predicted by plume theory. Furthermore, the compositional characteristics of a submarine lava flow in the eastern region of the archipelago provides evidence that Santiago may have once supported a centralized magmatic system, indicating a waning of magmatism at greater distances from the plume center. In addition, observations of source variations between closely spaced seamounts (<1 km), which do not follow predictable patterns, indicate that island-based sampling may lead to aliasing of the apparent scale and organization of mantle heterogeneities beyond their true length scales, which are likely smaller and less organized. From the evaluation of the geochemical and isotopic variations of seamount samples we show that geochemical domains observed geographically in the archipelago result from the disproportionate mixing of the principle components present in the Galápagos plume. Although, our evaluation of the monogenetic features is not comprehensive, this study exemplifies that the sampling of numerous small near-island volcanic features, even at a reconnaissance level, is required in order to accurately test second order predictions of plume theory.

Acknowledgments
Thanks to the crew of the M/V *Alucia* for skilled data and sample collection, and the Dalio Foundation for supporting the data and sample collection effort. We also thank the science party on the M/V *Alucia* cruise including Dan Fornari and Meghan Jones who assisted with data collection and post cruise data processing. We acknowledge the Dalio Foundation and the Ocean Exploration Trust for use of their assets, sample collection, as well as partial funding for post cruise research. We thank the Darwin Foundation for Facilitating research in the Galápagos and the Galápagos National Park and Ecuadorean Navy (Instituto Oceanográfico y Antártico de la Armada) for permission to operate in marine protected waters. We appreciate Josh Curtice for his analytical expertise in the He isotope lab at Woods Hole Oceanographic Institution, and the technical staff at the Peter Hooper Geoanalytical Facility at Washington State University for their assistance with the XRF analyses and data reduction. We thank Marion Lytle for her assistance in collecting trace element data at Boise State University. Finally, this work could not have been completed if it were not for the help of Emma McCully, Hannah Bercovici, Valerie Strasser, and Cecelia Wheeler for their assistance in sample preparation for various geochemical analyses. This work was carried out with funding from National Science Foundation Division of Ocean Sciences (OCE-1634952 to V. D. Wanless, OCE-1634685 to S. A. Soule). The authors have no competing interests to declare. We thank Sally Gibson and three anonymous reviewers for providing detailed and critical feedback on this manuscript.

Data Availability Statement

The data supporting this study are available within the article, Supporting Information and through EarthChem (https://doi.org/10.26022/IEDA/111730).

References

Abbott, K., & Richards, M. A. (2020). Elastic flexure of young, overlapping basaltic lava flows offshore the Galápagos and Hawaiian Islands: Observations, modeling, and thermal/chronological analysis. *Geochemistry, Geophysics, Geosystems*, *21*(3). https://doi.org/10.1029/2019GC008864

Abouchami, W., Hofmann, A. W., Galer, S. J. G., Frey, F. A., Eisele, J., & Feigenson, M. (2005). Lead isotopes reveal bilateral asymmetry and vertical continuity in the Hawaiian mantle plume. *Nature*, *434*(7035), 851.

Albarède, F., Luais, B., Fitton, G., Semet, M., Kaminski, E., Upton, B. G. J., et al (1997). The geochemical regimes of Piton de La Fournaise volcano (Réunion) during the last 530 000 years. *Journal of Petrology*, *38*(2), 171–201.

Allan, J. F., & Simkin, T. (2000). Fernandina Volcano's evolved, well-mixed basalts: Mineralogical and petrological constraints on the nature of the Galápagos plume. *Journal of Geophysical Research*, *105*(B3), 6017. https://doi.org/10.1029/1999JB900417

Anderson, M., Wanless, V. D., Schwartz, D. M., McCully, E., Fornari, D. J., Jones, M. R., et al. (2018). Submarine deep-water lava flows at the base of the western Galápagos platform. *Geochemistry, Geophysics, Geosystems*, *19*(10), 3945–3961. https://doi.org/10.1029/2018GC007632

Argus, D. F., Gordon, R. G., Heflin, M. B., Ma, C., Eanes, R. J., Willis, P., et al (2010). The angular velocities of the plates and the velocity of Earth's centre from space geodesy. *Geophysical Journal International*, *180*(3), 913–960.

Bagnardi, M., & Amelung, F. (2012). Space-geodetic evidence for multiple magma reservoirs and subvolcanic lateral intrusions at Fernandina Volcano, Galápagos Islands. *Journal of Geophysical Research*, *117*(B10). https://doi.org/10.1029/2012JB009465

Bagnardi, M., Amelung, F., & Poland, M. P. (2013). A new model for the growth of basaltic shields based on deformation of Fernandina volcano, Galápagos Islands. *Earth and Planetary Science Letters*, *377*, 358–366.

Bailey, K. (1976). Potassium-argon ages from the Galápagos Islands. *Science*, *192*(4238), 465–467.

Baitis, H. W., & Lindstrom, M. M. (1980). Geology, petrography, and petrology of Pinzon Island, Galápagos Archipelago. *Contributions to Mineralogy and Petrology*, *72*(4), 367–386.

Baitis, H. W., & Swanson, F. J. (1976). Ocean rise-like basalts within the Galápagos Archipelago. *Nature*, *259*(5540), 195–197.

Bianco, T. A., Ito, G., Becker, J. M., & Garcia, M. O. (2005). Secondary Hawaiian volcanism formed by flexural arch decompression. *Geochemistry, Geophysics, Geosystems*, *6*(8). https://doi.org/10.1029/2005GC000945

Bianco, T. A., Ito, G., van Hunen, J., Ballmer, M. D., & Mahoney, J. J. (2008). Geochemical variation at the Hawaiian hot spot caused by upper mantle dynamics and melting of a heterogeneous plume. *Geochemistry, Geophysics, Geosystems*, *9*(11). https://doi.org/10.1029/2008GC002111

Bianco, T. A., Ito, G., van Hunen, J., Ballmer, M. D., & Mahoney, J. J. (2011). Geochemical variations at intraplate hot spots caused by variable melting of a veined mantle plume. *Geochemistry, Geophysics, Geosystems*, *12*(7). https://doi.org/10.1029/2011GC003658

Blichert-Toft, J., & White, W. M. (2001). Hf isotope geochemistry of the Galápagos Islands. *Geochemistry, Geophysics, Geosystems*, *2*(9). https://doi.org/10.1029/2000GC000138

Bow, C. S., & Geist, D. J. (1992). Geology and petrology of Floreana Island, Galápagos Archipelago, Ecuador. *Journal of Volcanology and Geothermal Research*, *52*(1–3), 83–105.

Brenna, M., Cronin, S. J., Nemeth, K., Smith, I. E. M., & Sohn, Y. K. (2011). The influence of magma plumbing complexity on monogenetic eruptions, Jeju Island, Korea. *Terra Nova*, *23*(2), 70–75.

Buchs, D. M., Hoernle, K., Hauff, F., & Baumgartner, P. O. (2016). Evidence from accreted seamounts for a depleted component in the early Galápagos plume. *Geology*, *44*(5), 383–386.

Campbell, I. H. (2007). Testing the plume theory. *Chemical Geology*, *241*(3–4), 153–176.

Carey, B. S., Fisher, C. R., Leon, P. S., De, Roman, C., Raineault, N. A., Suarez, J., et al (2016). Oceanography. *Exploring the undersea world of the Galápagos Islands exploring the undersea world of the Galápagos Islands*, *29*(1), 32–34.

Carracedo, J. C. (1999). Growth, structure, instability and collapse of Canarian volcanoes and comparisons with Hawaiian volcanoes. *Journal of Volcanology and Geothermal Research*, *94*(1–4), 1–19.

Casalbore, D. (2018). Volcanic islands and seamounts. A.MicallefS.Krastel & A.Savini In *Submarine geomorphology* (pp. 333–347). New York City, New York: Springer.

Castillo, P. (1988). The Dupal anomaly as a trace of the upwelling lower mantle. *Nature*, *336*(6200), 667.

Chadwick, W. W., Jónsson, S., Geist, D. J., Poland, M., Johnson, D. J., Batt, S., et al. (2011). The May 2005 eruption of Fernandina volcano, Galápagos: The first circumferential dike intrusion observed by GPS and InSAR. *Bulletin of Volcanology*, *73*(6), 679–697. https://doi.org/10.1007/s00445-010-0433-0

Chaussidon, M., & Marty, B. (1995). Primitive boron isotope composition of the mantle. *Science*, *269*(5222), 383–386.

Christie, D. M. (2004). Major and trace element composition of basalts from the Galápagos Archipelago, Plume 2 cruise. *Version 1.0. Interdisciplinary Earth Data Alliance (IEDA)*. https://doi.org/10.1594/IEDA/100439

Christie, D. M., Duncan, R. A., McBirney, A. R., Richards, M. A., White, W. M., Harpp, K. S., et al. (1992). Drowned islands downstream from the Galápagos hotspot imply extended speciation times. *Nature*, *355*(6357), 246–248. https://doi.org/10.1038/355246a0

Clague, D. A., & Dalrymple, G. B. (1987). The Hawaiian-Emperor volcanic chain. Part I. Geologic evolution. *Volcanism in Hawaii*, *1*, 5–54.

Clague, D. A., Moore, J. G., & Reynolds, J. R. (2000). Formation of submarine flat-topped volcanic cones in Hawai'i. *Bulletin of Volcanology*, *62*(3), 214–233. https://doi.org/10.1007/s004450000088

Clague, D. A., & Sherrod, D. R. (2014). Growth and degradation of Hawaiian volcanoes. *Geological Survey Professional Paper*, *1801*, 97–146.

Cleary, Z., Schwartz, D. M., Mittelstaedt, E., & Harpp, K. (2020). Dynamic magma storage at near-ridge hotspots: Evidence from new Galápagos gravity data. *Geochemistry, Geophysics, Geosystems*, *21*(3). https://doi.org/10.1029/2019GC008722

Colin, A., Burnard, P. G., Graham, D. W., & Marrocchi, Y. (2011). Plume–ridge interaction along the Galápagos spreading center: Discerning between gas loss and source effects using neon isotopic compositions and ^{4}He–$^{40}Ar*$–CO_2 relative abundances. *Geochimica et Cosmochimica Acta*, *75*(4), 1145–1160.

Courtillot, V., Davaille, A., Besse, J., & Stock, J. (2003). Three distinct types of hotspots in the Earth's mantle. *Earth and Planetary Science Letters*, *205*(3), 295–308.

Cousens, B. L., & Clague, D. A. (2015). Shield to rejuvenated stage volcanism on Kauai and Niihau, Hawaiian Islands. *Journal of Petrology*, *56*(8), 1547–1584.

Cox, A., & Dalrymple, G. B. (1966). Palaeomagnetism and potassium-argon ages of some volcanic rocks from the Galápagos Islands. *Nature*, *209*(5025), 776–777.

Cushman, B., Sinton, J., Ito, G., & Dixon, J. E. (2004). Glass compositions, plume-ridge interaction, and hydrous melting along the Galápagos Spreading Center, 90.5° W to 98° W. *Geochemistry, Geophysics, Geosystems*, *5*(8). https://doi.org/10.1029/2004GC000709

Detrick, R. S., Sinton, J. M., Ito, G., Canales, J. P., Behn, M., Blacic, T., et al (2002). Correlated geophysical, geochemical, and volcanological manifestations of plume-ridge interaction along the Galápagos Spreading Center. *Geochemistry, Geophysics, Geosystems*, *3*(10), 1–14. https://doi.org/10.1029/2002GC000350

Devey, C. W., Lackschewitz, K. S., Mertz, D. F., Bourdon, B., Cheminée, J.-L., Dubois, J., et al (2003). Giving birth to hotspot volcanoes: Distribution and composition of young seamounts from the seafloor near Tahiti and Pitcairn islands. *Geology*, *31*(5), 395–398.

Feighner, M. A., & Richards, M. A. (1994). Lithospheric structure and compensation mechanisms of the Galápagos Archipelago. *Journal of Geophysical Research*, *99*, 6711–6729. https://doi.org/10.1029/93JB03360

Fisher, C. M., McFarlane, C. R. M., Hanchar, J. M., Schmitz, M. D., Sylvester, P. J., Lam, R., et al. (2011). Sm–Nd isotope systematics by laser ablation-multicollector-inductively coupled plasma mass spectrometry: Methods and potential natural and synthetic reference materials. *Chemical Geology*, *284*(1–2), 1–20.

Fisk, M. R., Bence, A. E., & Schilling, J.-G. (1982). Major element chemistry of Galapagos Rift Zone magmas and their phenocrysts. *Earth and Planetary Science Letters*, *61*(1), 171–189. https://doi.org/10.1016/0012-821x(82)90050-4

Garcia, M. O., Hulsebosch, T. P., & Rhodes, J. M. (1995). Olivine-rich submarine basalts from the southwest rift zone of Mauna Loa volcano: Implications for magmatic processes and geochemical evolution. *Mauna Loa Revealed: Structure, Composition, History, and Hazards*, *92*, 219–239.

Gazel, E., Trela, J., Bizimis, M., Sobolev, A., Batanova, V., Class, C., et al. (2018). Long-lived source heterogeneities in the Galápagos mantle plume. *Geochemistry, Geophysics, Geosystems*, *19*(8), 2764–2779. https://doi.org/10.1029/2017GC007338

Geist, D. J., Bergantz, G., Chadwick, W. W., & Harpp, K. S. (2014). Galápagos magma chambers. In et K. S.HarppE.MittelstaedtN.d'Ozouville & D. W,.Graham al. *The Galápagos: A natural Laboratory for the Earth sciences. American geophysical Union* (pp. 55–70). Washington, DC, USA: John Wiley & Sons, Inc.

Geist, D., Diefenbach, B. A., Fornari, D. J., Kurz, M. D., Harpp, K., & Blusztajn, J. (2008). Construction of the Galápagos platform by large submarine volcanic terraces. *Geochemistry, Geophysics, Geosystems*, *9*(3). https://doi.org/10.1029/2007GC001795

Geist, D. J., Fornari, D. J., Kurz, M. D., Harpp, K. S., Adam Soule, S., Perfit, M. R., et al. (2006). Submarine Fernandina: Magmatism at the leading edge of the Galápagos hot spot. *Geochemistry, Geophysics, Geosystems*, *7*(12). https://doi.org/10.1029/2006GC001290

Geist, D. J., Harpp, K. S., Naumann, T. R., Poland, M., Chadwick, W. W., Hall, M., et al. (2008). The 2005 eruption of Sierra Negra volcano, Galápagos, Ecuador. *Bulletin of Volcanology*, *70*(6), 655–673.

Geist, D., Howard, K. A., Jellinek, A. M., & Rayder, S. (1994). The volcanic history of Volcán Alcedo, Galápagos Archipelago: A case study of rhyolitic oceanic volcanism. *Bulletin of Volcanology*, *56*(4), 243–260.

Geist, D., Howard, K. A., & Larson, P. (1995). The generation of oceanic rhyolites by crystal fractionation: The basalt-rhyolite association at Volcan Alcedo, Galápagos Archipelago. *Journal of Petrology*, *36*(4), 965–982.

Geist, D. J., McBirney, A. R., & Duncan, R. A. (1985). Geology of Santa Fe island: The oldest Galápagos volcano. *Journal of Volcanology and Geothermal Research*, *26*(3–4), 203–212.

Geist, D., Naumann, T., & Larson, P. (1998). Evolution of Galápagos magmas: Mantle and crustal fractionation without assimilation. *Journal of Petrology*, *39*(5), 953–971. https://doi.org/10.1093/petrology/39.5.953

Geist, D. J., Naumann, T. R., Standish, J. J., Kurz, M. D., Harpp, K. S., White, W. M., et al. (2005). Wolf Volcano, Galápagos Archipelago: Melting and magmatic evolution at the margins of a mantle plume. *Journal of Petrology*, *46*(11), 2197–2224.

Geist, D., Snell, H., Snell, H., Goddard, C., & Kurz, M. D. (2014). A paleogeographic model of the Galápagos Islands and biogeographical and evolutionary implications. K. S.HarppE.MittelstaedtN.d'Ozouville & D. W.Graham In *The Galápagos: A natural laboratory for the Earth sciences. American geophysical Union*, (pp. 145–166). Washington, DC, USA: John Wiley & Sons, Inc.

Geist, D., White, W. M., Albarede, F., Harpp, K., Reynolds, R., Blichert-Toft, J., et al. (2002). Volcanic evolution in the Galápagos: The dissected shield of Volcan Ecuador. *Geochemistry, Geophysics, Geosystems*, *3*(10). https://doi.org/10.1029/2002GC000355

Geist, D. J., White, W. M., & McBirney, A. R. (1988). Plume-asthenosphere mixing beneath the Galápagos Archipelago. *Nature*, *333*, 657–660.

Geldmacher, J., Hanan, B. B., Blichert-Toft, J., Harpp, K., Hoernle, K., Hauff, F., et al (2003). Hafnium isotopic variations in volcanic rocks from the Caribbean Large Igneous Province and Galápagos hot spot tracks. *Geochemistry, Geophysics, Geosystems*, *4*(7).

Gibson, S. A., & Geist, D.. (2010). Geochemical and geophysical estimates of lithospheric thickness variation beneath Galápagos. *Earth and Planetary Science Letters*, *300*(3–4), 275–286. https://doi.org/10.1016/j.epsl.2010.10.002

Gibson, S. A., Geist, D. G., Day, J. A., & Dale, C. W. (2012). Short wavelength heterogeneity in the Galápagos plume: Evidence from compositionally diverse basalts on Isla Santiago. *Geochemistry Geophysics Geosystems*, *13*, Q09007. https://doi.org/10.1029/2012GC004244

Gibson, S. A., Geist, D. J., & Richards, M. A. (2015). Mantle plume capture, anchoring, and outflow during Galápagos plume-ridge interaction. *Geochemistry, Geophysics, Geosystems*, *16*(5), 1634–1655. https://doi.org/10.1002/2015GC005723

Graham, D. W., Christie, D. M., Harpp, K. S., & Lupton, J. E. (1993). Mantle plume helium in submarine basalts from the Galápagos platform. *Science*, *262*(5142), 2023–2026.

Greene, A. R., Garcia, M. O., Weis, D., Ito, G., Kuga, M., Robinson, J., et al. (2010). Low-productivity Hawaiian volcanism between Kaua ʻi and O ʻahu. *Geochemistry, Geophysics, Geosystems*, *11*(11). https://doi.org/10.1029/2010GC003233

Handley, H. K., Turner, S., Berlo, K., Beier, C., & Saal, A. E. (2011). Insights into the Galápagos plume from uranium-series isotopes of recently erupted basalts. *Geochemistry, Geophysics, Geosystems*, *12*(9). https://doi.org/10.1029/2011GC003676

Harpp, K. S., Fornari, D. J., Geist, D. J., & Kurz, M. D. (2003). Genovesa submarine ridge: A manifestation of plume-ridge interaction in the northern Galápagos islands. *Geochemistry, Geophysics, Geosystems*, *4*(9). https://doi.org/10.1029/2003GC000531

Harpp, K., Fornari, D., Geist, D. J., & Kurz, M. D. (2014). The geology and geochemistry of Isla Floreana, Galápagos: A different type of late stage ocean island volcanism. In *The Galápagos: A natural laboratory for the Earth sciences. American geophysical Union*. Vol. 204 (pp. 71–118). Washington. DC, USA: John Wiley & Sons, Inc.

Harpp, K., & Geist, D. (2002). Wolf–Darwin lineament and plume–ridge interaction in northern Galápagos. *Geochemistry, Geophysics, Geosystems*, *3*(11), 1–19. https://doi.org/10.1029/2002GC000370

Harpp, K. S., & Geist, D. J. (2018). The evolution of Galápagos volcanoes: An alternative perspective. *Frontiers in Earth Science*, *6*, 50.

Harpp, K. S., Hall, P. S., & Jackson, M. G. (2014a).Galápagos and Easter: A tale of two hotspots. In *The Galápagos: A natural laboratory for the Earth sciences. American geophysical Union*. Vol. 204 (pp. 27–40). Washington, DC, USA: John Wiley & Sons, Inc.

Harpp, K. S., & White, W. M. (2001). Tracing a mantle plume: Isotopic and trace element variations of Galápagos seamounts. *Geochemistry, Geophysics, Geosystems*, *2*(2000). https://doi.org/10.1029/2000GC000137

Hart, S. R., Hauri, E. H., Oschmann, L. A., & Whitehead, J. A. (1992). Mantle plumes and entrainment: Isotopic evidence. *Science*, *256*(5056), 517–520.

Hauff, F., Hoernle, K., Tilton, G., Graham, D. W., & Kerr, A. C. (2000). Large volume recycling of oceanic lithosphere over short time scales: Geochemical constraints from the Caribbean Large Igneous Province. *Earth and Planetary Science Letters*, *174*(3–4), 247–263.

Hedge, C. E. (1978). Strontium isotopes in basalts from the Pacific Ocean basin. *Earth and Planetary Science Letters*, *38*(1), 88–94.

Hoernle, K., Rohde, J., Hauff, F., Garbe-Schönberg, D., Homrighausen, S., Werner, R., et al. (2015). How and when plume zonation appeared during the 132 Myr evolution of the Tristan Hotspot. *Nature Communications*, *6*, 7799.

Hoernle, K., Werner, R., Morgan, J. P., Garbe-Schönberg, D., Bryce, J., & Mrazek, J. (2000). Existence of complex spatial zonation in the Galápagos plume. *Geology*, *28*(5), 435–438.

Hofmann, A. W. (1997). Mantle geochemistry: The message from oceanic volcanism. *Nature*, *385*(6613), 219.

Hooft, E. E. E., Toomey, D. R., & Solomon, S. C. (2003). Anomalously thin transition zone beneath the Galápagos hotspot. *Earth and Planetary Science Letters*, *216*(1), 55–64.

Ito, G., & Bianco, T. (2014). Patterns in Galápagos magmatism arising from the upper mantle dynamics of plume-ridge interaction. K. S.HarppE.MittelstaedtN.d'Ozouville & D. W.Graham*The Galápagos: A natural laboratory for the Earth sciences. American geophysical Union*, (245–262). Washington, DC, USA: John Wiley & Sons.

Jackson, M. G., & Carlson, R. W. (2012). Homogeneous superchondritic 142Nd/144Nd in the mid-ocean ridge basalt and ocean island basalt mantle. *Geochemistry, Geophysics, Geosystems*, *13*(6). https://doi.org/10.1029/2012GC004114

Jochum, K. P., Weis, U., Schwager, B., Stoll, B., Wilson, S. A., Haug, G. H., et al (2016). Reference values following ISO guidelines for frequently requested rock reference materials. *Geostandards and Geoanalytical Research*, *40*(3), 333–350.

Johnson, D. M., Hooper, P. R., & Conrey, R. M. (1999). XRF analysis of rocks and minerals for major and trace elements on a single low dilution Li-tetraborate fused bead. *Advances in X-Ray Analysis*, *41*(C), 843–867.

Jones, T. D., Davies, D. R., Campbell, I. H., Iaffaldano, G., Yaxley, G., Kramer, S. C., et al. (2017). The concurrent emergence and causes of double volcanic hotspot tracks on the Pacific plate. *Nature*, *545*(7655), 472.

Jones, T. D., Davies, D. R., Campbell, I. H., Wilson, C. R., & Kramer, S. C. (2016). Do mantle plumes preserve the heterogeneous structure of their deep-mantle source?. *Earth and Planetary Science Letters*, *434*, 10–17.

Kelley, K. A., Plank, T., Ludden, J., & Staudigel, H. (2003). Composition of altered oceanic crust at ODP Sites 801 and 1149. *Geochemistry, Geophysics, Geosystems*, *4*(6). https://doi.org/10.1029/2002GC000435

Kelley, K. A., Kingsley, R., & Schilling, J. (2013). Composition of plume-influenced mid-ocean ridge lavas and glasses from the Mid-Atlantic Ridge, East Pacific Rise, Galápagos Spreading Center, and Gulf of Aden. *Geochemistry, Geophysics, Geosystems*, *14*(1), 223–242. https://doi.org/10.1002/ggge.20049

Kokfelt, T. F., Lundstrom, C., Hoernle, K., Hauff, F., & Werner, R. (2005). Plume–ridge interaction studied at the Galápagos spreading center: Evidence from 226Ra–230Th–238U and 231Pa–235U isotopic disequilibria. *Earth and Planetary Science Letters*, *234*(1–2), 165–187.

Koleszar, A. M., Saal, A. E., Hauri, E. H., Nagle, A. N., Liang, Y., & Kurz, M. D. (2009). The volatile contents of the Galápagos plume; evidence for H_2O and F open system behavior in melt inclusions. *Earth and Planetary Science Letters*, *287*(3–4), 442–452. https://doi.org/10.1016/j.epsl.2009.08.029

Korkisch, J., & Worsfold, P. J. (1990). *Handbook of ion exchange resins: their application to inorganic analytical chemistry*. Boca Raton, FL: CRC Press.

Kurz, M. D. (1986a). In situ production of terrestrial cosmogenic helium and some applications to geochronology. *Geochimica et Cosmochimica Acta*, *50*(12), 2855–2862.

Kurz, M. D. (1986b). Cosmogenic helium in a terrestrial igneous rock. *Nature*, *320*(6061), 435.

Kurz, M. D., Curtice, J., Fornari, D., Geist, D., & Moreira, M. (2009). Primitive neon from the center of the Galápagos hotspot. *Earth and Planetary Science Letters*, *286*(1–2), 23–34.

Kurz, M. D., & Geist, D. (1999). Dynamics of the Galápagos hotspot from helium isotope geochemistry. *Geochimica et Cosmochimica Acta*, *63*(23–24), 4139–4156.

Kurz, M. D., Kenna, T. C., Lassiter, J. C., & DePaolo, D. J. (1996). Helium isotopic evolution of Mauna Kea Volcano: First results from the 1-km drill core. *Journal of Geophysical Research*, *101*(B5), 11781–11791. https://doi.org/10.1029/95JB03345

Kurz, M. D., Rowland, S., Curtice, J., Saal, A., & Naumann, T. (2014). Eruption rates for Fernandina volcano: A new chronology at the Galápagos hotspot center. K. S.HarppE.MittelstaedtN.d'Ozouville & D. W.Graham In *The Galápagos: A natural laboratory for the Earth sciences. American geophysical Union*, Vol. 204 (pp. 41–54). Washington, DC, USA: John Wiley & Sons, Inc.

Kurz, G. A., Schmitz, M. D., Northrup, C. J., & Vallier, T. L. (2017). Isotopic compositions of intrusive rocks from the Wallowa and Olds Ferry arc terranes of northeastern Oregon and western Idaho: Implications for Cordilleran evolution, lithospheric structure, and Miocene magmatism. *Lithosphere*, *9*(2), 235–264.

Le Corvec, N., Menand, T., & Lindsay, J. (2013). Interaction of ascending magma with pre-existing crustal fractures in monogenetic basaltic volcanism: An experimental approach. *Journal of Geophysical Research: Solid Earth*, *118*(3), 968–984. https://doi.org/10.1002/jgrb.50142

Liang, Y.-H., Halliday, A. N., Siebert, C., Fitton, J. G., Burton, K. W., Wang, K.-L., et al. (2017). Molybdenum isotope fractionation in the mantle. *Geochimica et Cosmochimica Acta*, *199*, 91–111.

Lyons, J., Geist, D., Harpp, K., Diefenbach, B., Olin, P., & Vervoort, J. (2007). Crustal growth by magmatic overplating in the Galápagos. *Geology*, *35*(6), 511–514.

Lytle, M. L., Kelley, K. A., Hauri, E. H., Gill, J. B., Papia, D., & Arculus, R. J. (2012). Tracing mantle sources and Samoan influence in the northwestern Lau back-arc basin. *Geochemistry, Geophysics, Geosystems*, *13*(10) https://doi.org/10.1029/2012GC004233

MacDonald, G. A., & Katsura, T. (1964). Chemical composition of Hawaiian lavas. *Journal of Petrology*, *5*(1), 82–133.

Macdonald, R., Smith, R. L., & Thomas, J. E. (1992). Chemistry of the subalkalic silicic obsidians. *USGS Professional Paper*, Washington, DC: United States Printing Office.

Marty, B., & Humbert, F. (1997). Nitrogen and argon isotopes in oceanic basalts. *Earth and Planetary Science Letters*, *152*(1–4), 101–112.

Mazza, S. E., Gazel, E., Bizimis, M., Moucha, R., Béguelin, P., Johnson, E. A., et al (2019). Sampling the volatile-rich transition zone beneath Bermuda. *Nature*, *569*(7756), 398.

McBirney, A. R., Cullen, A. B., Geist, D., Vicenzi, E. P., Duncan, R. A., Hall, M. L., et al. (1985). The Galápagos volcano Alcedo: A unique ocean caldera. *Journal of Volcanology and Geothermal Research*, *26*(1–2), 173–177.

McBirney, A. R., & Williams, H. (1969). Geology and petrology of the Galápagos islands. *Geological Society of America Memoir*, *118*, 1–197.

McDonough, W. F., & Sun, S.-S. (1995). The composition of the Earth. *Chemical Geology*, *120*(3–4), 223–253.

Mittelstaedt, E., Soule, S., Harpp, K., Fornari, D., McKee, C., Tivey, M., et al (2012). Multiple expressions of plume-ridge interaction in the Galápagos: Volcanic lineaments and ridge jumps. *Geochemistry, Geophysics, Geosystems*, *13*(5), Q05018. https://doi.org/10.1029/2012GC004093

Moore, J. G., Clague, D. A., & Normark, W. R. (1982). Diverse basalt types from Lō'ihi seamount. *Hawaii. Geology*, *10*(2), 88–92.

Morgan, W. J. (1971). Convection plumes in the lower mantle. *Nature*, *230*(5288), 42.

Muirhead, J. D., Eaton, V., Re, G., White, J. D. L., & Ort, M. H. (2016). Monogenetic volcanoes fed by interconnected dikes and sills in the Hopi Buttes volcanic field, Navajo Nation, USA. *Bulletin of Volcanology*, *78*(2), 11.

Naumann, T., Geist, D., & Kurz, M. (2002). Petrology and geochemistry of Volcan cerro Azul: Petrologic diversity among the western Galápagos volcanoes. *Journal of Petrology*, *43*(5), 859–883.

Needham, A. J., Lindsay, J. M., Smith, I. E. M., Augustinus, P., & Shane, P. A. (2011). Sequential eruption of alkaline and sub-alkaline magmas from a small monogenetic volcano in the Auckland Volcanic Field, New Zealand. *Journal of Volcanology and Geothermal Research*, *201*(1–4), 126–142.

Nusbaum, R. L., Colgan, M. W., Lawton, D. E., & Glascock, M. D. (1991). Mineralogic constraints on the magmatic history of Volcán Darwin flank lava at Urvina Bay, Islá Isabela, Galápagos islands. *Journal of Volcanology and Geothermal Research*, *47*(3–4), 359–366.

Peterson, M. E., Saal, A. E., Kurz, M. D., Hauri, E. H., Blusztajn, J. S., Harpp, K. S., et al (2017). Submarine basaltic glasses from the Galápagos Archipelago: Determining the volatile budget of the mantle plume. *Journal of Petrology*, *58*(7), 1419–1450.

Peterson, M. E., Saal, A. E., Nakamura, E., Kitagawa, H., Kurz, M. D., & Koleszar, A. M. (2014). Origin of the "ghost plagioclase" signature in Galápagos melt inclusions: New evidence from Pb isotopes. *Journal of Petrology*, *55*(11), 2193–2216.
Pringle, E. A., Moynier, F., Savage, P. S., Jackson, M. G., Moreira, M., & Day, J. M. D. (2016). Silicon isotopes reveal recycled altered oceanic crust in the mantle sources of ocean island basalts. *Geochimica et Cosmochimica Acta*, *189*, 282–295.
Puzankov, Y. M., & Bobrov, V. A. (1997). Geochemistry of the volcanic rocks from Easter and Sala y Gomez islands. *Geochemistry International*, *35*(7), 609–619.
Raquin, A., & Moreira, M. (2009). Atmospheric 38Ar/36Ar in the mantle: Implications for the nature of the terrestrial parent bodies. *Earth and Planetary Science Letters*, *287*(3–4), 551–558.
Rasoazanamparany, C., Widom, E., Valentine, G. A., Smith, E. I., Cortés, J. A., Kuentz, D., et al. (2015). Origin of chemical and isotopic heterogeneity in a mafic, monogenetic volcanic field: A case study of the Lunar Crater Volcanic field, Nevada. *Chemical Geology*, *397*, 76–93.
Reynolds, R. W., & Geist, D. J. (1995). Petrology of lavas from Sierra Negra volcano, Isabela island, Galápagos Archipelago. *Journal of Geophysical Research*, *100*(B12), 24537–24553. https://doi.org/10.1029/95JB02809
Righter, K., Chesley, J. T., Geist, D., & Ruiz, J. (1998). Behavior of Re during magma fractionation: An example from Volcan Alcedo, Galápagos. *Journal of Petrology*, *39*(4), 785–795.
Ryan, W. B. F., Carbotte, S. M., Coplan, J. O., O'Hara, S., Melkonian, A., Arko, R., et al (2009). Global multi-resolution topography synthesis. *Geochemistry, Geophysics, Geosystems*, *10*(3). https://doi.org/10.1029/2008GC002332
Saal, A. E., Kurz, M. D., Hart, S. R., Blusztajn, J. S., Blichert-Toft, J., Liang, Y., et al. (2007). The role of lithospheric gabbros on the composition of Galápagos lavas. *Earth and Planetary Science Letters*, *257*(3), 391–406.
Schwartz, D. M., Soule, S. A., Wanless, V. D., & Jones, M. R. (2018a). Identification of erosional terraces on seamounts: Implications for interisland connectivity and subsidence in the Galápagos Archipelago. *Frontiers in Earth Science*, *6*, 88.
Schwartz, D. M., Wanless, V. D., Berg, R., Jones, M., Fornari, D. J., Soule, S. A., et al (2018b). Petrogenesis of alkalic seamounts on the Galápagos platform. *Deep-Sea Research Part II: Topical Studies in Oceanography*, *150*(2017), 170–180. https://doi.org/10.1016/j.dsr2.2017.09.019
Shimizu, H., Masuda, A., & Masui, N. (1981). Rare-earth element geochemistry of volcanic and related rocks from the Galápagos Islands. *Geochemical Journal*, *15*(2), 81–93.
Schilling, J., Fontignie, D., Blichert-Toft, J., Kingsley, R., Tomza, U. (2003). Pb-Hf-Nd-Sr isotope variations along the Galápagos Spreading Center (101°-83°W): Constraints on the dispersal of the Galápagos mantle plume. *Geochemistry, Geophysics, Geosystems*, *4*(10). https://doi.org/10.1029/2002gc000495
Siebert, L., Simkin, T., & Kimberly, P. (2011). *Volcanoes of the world*, Los Angeles, CA: University of California Press.
Silva, I. G., Weis, D., Barling, J., & Scoates, J. S. (2009). Leaching systematics and matrix elimination for the determination of high-precision Pb isotope compositions of ocean island basalts. *Geochemistry, Geophysics, Geosystems*, *10*(8). https://doi.org/10.1029/2009GC002537
Simkin, T., & Howard, K. A. (1970). Caldera collapse in the Galápagos islands, 1968. *Science*, *169*(3944), 429–437.
Sinton, C. W., Harpp, K. S., & Christie, D. M. (2014). A preliminary survey of the northeast seamounts, galápagos platform. *The Galápagos: A Natural Laboratory for the Earth Sciences*, *204*, 335.
Smith, I. E. M., & Németh, K. (2017). Source to surface model of monogenetic volcanism: A critical review. *Geological Society, London, Special Publications*, *446*(1), 1–28.
Sousa, J., Kohn, M. J., Schmitz, M. D., Northrup, C. J., & Spear, F. S. (2013). Strontium isotope zoning in garnet: Implications for metamorphic matrix equilibration, geochronology and phase equilibrium modelling. *Journal of Metamorphic Geology*, *31*(4), 437–452.
Standish, J., Geist, D., Harpp, K., & Kurz, M. D. (1998). The emergence of a Galápagos shield volcano, Roca Redonda. *Contributions to Mineralogy and Petrology*, *133*(1–2), 136–148.
Stracke, A., & Bourdon, B. (2009). The importance of melt extraction for tracing mantle heterogeneity. *Geochimica et Cosmochimica Acta*, *73*(1), 218–238.
Swanson, F. J., Baitis, H. W., Lexa, J., & Dymond, J. (1974). Geology of Santiago, Rábida, and Pinzón islands, Galápagos. *Geological Society of America Bulletin*, *85*(11), 1803–1810.
Tanaka, T., Togashi, S., Kamioka, H., Amakawa, H., Kagami, H., Hamamoto, T., et al (2000). JNdi-1: A neodymium isotopic reference in consistency with LaJolla neodymium. *Chemical Geology*, *168*(3–4), 279–281.
Teasdale, R., Geist, D., Kurz, M., & Harpp, K. (2005). 1998 eruption at Volcán cerro Azul, Galápagos islands: I. syn-eruptive petrogenesis. *Bulletin of Volcanology*, *67*(2), 170–185.
Thirlwall, M. F. (1982). A triple-filament method for rapid and precise analysis of rare-earth elements by isotope dilution. *Chemical Geology*, *35*(1–2), 155–166.
Thirlwall, M. F. (1991). Long-term reproducibility of multicollector Sr and Nd isotope ratio analysis. *Chemical Geology: Isotope Geoscience Section*, *94*(2), 85–104.
Trela, J., Vidito, C., Gazel, E., Herzberg, C., Class, C., Whalen, W., et al (2015). Recycled crust in the Galápagos plume source at 70 Ma: Implications for plume evolution. *Earth and Planetary Science Letters*, *425*, 268–277.
Turner, S., Regelous, M., Hawkesworth, C., & Rostami, K. (2006). Partial melting processes above subducting plates: Constraints from 231Pa–235U disequilibria. *Geochimica et Cosmochimica Acta*, *70*(2), 480–503.
Villagómez, D. R., Toomey, D. R., Geist, D. J., Hooft, E. E. E., & Solomon, S. C. (2014). Mantle flow and multistage melting beneath the Galápagos hotspot revealed by seismic imaging. *Nature Geoscience*, *7*(2), 151.
Villagómez, D. R., Toomey, D. R., Hooft, E. E. E., & Solomon, S. C. (2007). Upper mantle structure beneath the Galápagos Archipelago from surface wave tomography. *Journal of Geophysical Research*, *112*(B7). https://doi.org/10.1029/2006JB004672
Walker, G. P. L. (2000). Basaltic volcanoes and volcanic systems. H. Sigurdsson & *Encyclopedia of Volcanoes*, 283–289). Cambridge, Massachusetts: Academic Press.
Wanless, V. D., Garcia, M. O., Rhodes, J. M., Weis, D., & Norman, M. D. (2006a). Shield-stage alkalic volcanism on Mauna Loa volcano, Hawaii. *Journal of Volcanology and Geothermal Research*, *151*(1–3), 141–155.
Wanless, V. D., Garcia, M. O., Trusdell, F. A., Rhodes, J. M., Norman, M. D., Weis, D., et al (2006b). Submarine radial vents on Mauna Loa Volcano, Hawai'i. *Geochemistry, Geophysics, Geosystems*, *7*(5). https://doi.org/10.1029/2005GC001086
Watson, S., & McKenzie, D. (1991). Melt Generation by Plumes: A Study of Hawaiian Volcanism. *Journal of Petrology*, *32*(3), 501–537. https://doi.org/10.1093/petrology/32.3.501
Weis, D., Garcia, M. O., Rhodes, J. M., Jellinek, M., & Scoates, J. S. (2011). Role of the deep mantle in generating the compositional asymmetry of the Hawaiian mantle plume. *Nature Geoscience*, *4*(12), 831.

Werner, R., Hoernle, K., Barckhausen, U., & Hauff, F. (2003). Geodynamic evolution of the Galápagos hot spot system (Central East Pacific) over the past 20 my: Constraints from morphology, geochemistry, and magnetic anomalies. *Geochemistry, Geophysics, Geosystems*, *4*(12). https://doi.org/10.1029/2003GC000576

Werner, R., Hoernle, K., van den Bogaard, P., Ranero, C., von Huene, R., & Korich, D. (1999). Drowned 14-my-old Galápagos Archipelago off the coast of Costa Rica: Implications for tectonic and evolutionary models. *Geology*, *27*(6), 499–502.

White, W. M., & Hofmann, A. W. (1978). Geochemistry of the Galápagos islands: Implications for mantle dynamics and evolution. *Year Book - Carnegie Institution of Washington*, *77*, 596–606.

White, W. M., McBirney, A. R., & Duncan, R. A. (1993). Petrology and geochemistry of the Galápagos Islands: Portrait of a pathological mantle plume. *Journal of Geophysical Research*, *98*(B11), 19533–19563. https://doi.org/10.1029/93JB02018

Wilson, J. T. (1963). A possible origin of the Hawaiian Islands. *Canadian Journal of Physics*, *41*(6), 863–870.

Wilson, E. L. (2013). The geochemical evolution of Santa Cruz island, Galápagos archipelago. *Master's Thesis*, Moscow, Idaho: University of Idaho.

Wood, C. A. (1979). Monogenetic volcanoes of the terrestrial planets. In *Lunar and Planetary Science Conference Proceedings* (Vol. 10, pp. 2815–2840).

Yi, W., Halliday, A. N., Alt, J. C., Lee, D., Rehkämper, M., Garcia, M. O., et al (2000). Cadmium, indium, tin, tellurium, and sulfur in oceanic basalts: Implications for chalcophile element fractionation in the Earth. *Journal of Geophysical Research*, *105*(B8), 18927–18948. https://doi.org/10.1029/2000JB900152